EHD2-mediated restriction of caveolar dynamics regulates cellular lipid uptake

Claudia Matthäus[1,10*], Ines Lahmann[2,10], Séverine Kunz[3], Wenke Jonas[4], Arthur Alves Melo[1], Martin Lehmann[5], Elin Larsson[6], Richard Lundmark[6], Matthias Kern[7], Matthias Blüher[7], Dominik N. Müller[8], , Volker Haucke[5], Annette Schürmann[4], Carmen Birchmeier[2], Oliver Daumke[1,9,*]

[1] Crystallography, Max-Delbrück-Center for Molecular Medicine, Berlin, Germany

[2] Signal Transduction/Developmental Biology, Max-Delbrück-Center for Molecular Medicine, Berlin, Germany

[3] Electron Microscopy Facility, Max-Delbrück-Center for Molecular Medicine, Berlin, Germany

[4] Experimental Diabetology, German Institute of Human Nutrition, German Center for Diabetes Research, München-Neuherberg, Potsdam, Germany

[5] Dept. of Molecular Pharmacology & Cell Biology and Imaging Core Facility, Leibniz-Forschungsinstitut für Molekulare Pharmakologie, Berlin, Germany

[6] Integrative Medical Biology, Umeå University, 901 87 Umeå, Sweden

[7] Department of Medicine, University of Leipzig, Leipzig, Germany

[8] Experimental & Clinical Research Center, a cooperation between Charité Universitätsmedizin Berlin and Max Delbrück Center for Molecular Medicine, Berlin, Germany

[9] Institute of Chemistry and Biochemistry, Freie Universität Berlin, Takustrasse 6, 14195 Berlin, Germany

[10] These authors contributed equally

*Corresponding authors

Correspondence: claudia.matthaeus@mdc-berlin.de; oliver.daumke@mdc-berlin.de

Abstract

Eps15-homology domain containing protein 2 (EHD2) is a dynamin-related ATPase located at the neck of caveolae, but its physiological function has remained unclear. Here, we found that global genetic ablation of EHD2 in mice led to increased fat accumulation. This organismic phenotype was paralleled at the cellular level by increased lipid uptake via a caveolae-, dynamin- and CD36-dependent pathway, an elevated number of detached caveolae and higher caveolar mobility. Furthermore, EHD2 expression itself was down-regulated in the visceral fat of two obese mouse models and obese patients. Our data suggest that EHD2 controls a cell-autonomous, caveolae-dependent lipid uptake pathway and suggest that low EHD2 expression levels are linked to obesity.

Keywords: EHD2, caveolae, fatty acid uptake, lipid metabolism, obesity

39 **Introduction**

40 Caveolae are small membrane invaginations of the plasma membrane that are abundantly found
41 in adipocytes, endothelial and muscle cells (1). They have been implicated in the regulation of membrane
42 tension (2, 3), in mediating lipid metabolism (4), or in acting as distinct sites for specific and highly
43 regulated signaling cascades such as the endothelial nitric oxide synthase (eNOS)-nitric oxide (NO)
44 pathway (5). The characteristically shaped caveolar bulb has a typical diameter of 50 - 100 nm and is
45 connected to the cell surface via a narrow neck region. The integral membrane protein Caveolin (with
46 three isoforms in human, Cav1-3) and the peripheral membrane protein Cavin (with four isoforms in
47 human, Cavin1-4) build a mesh-like coat around the caveolar bulb (6–10). In addition, BAR domain
48 containing proteins of the PACSIN/syndapin family (PACSIN1-3 in human) participate in the biogenesis of
49 caveolae (11–13).

50 Loss of Cav1/Cav3 or Cavin1 results in a complete lack of caveolae from the plasma membrane (4,
51 14, 15). Cav1 KO mice suffer from cardiomyopathy, pulmonary hypertension, endothelium-dependent
52 relaxation problems and defective lipid metabolism (1). In agreement with the latter, Cav1 KO mice are
53 resistant to high fat diet-induced obesity (16) and display smaller white adipocytes and fat pads (17).
54 Furthermore, increased levels of triglycerides and fatty acids are found in blood plasma samples obtained
55 from Cav1 KO mice suggesting a reduced cellular uptake of fatty acids (16). A similar metabolic phenotype
56 was found in mice lacking Cavin1 (4, 18). Conversely, overexpression of Cav1 in adipocytes results in an
57 increased number of caveolae, enhanced fat accumulation, enlarged adipocytes and lipid droplets (LDs)
58 (19). These results suggest that caveolae are involved in lipid accumulation in adipocytes and may
59 promote fatty acid uptake (20). However, the molecular mechanisms of caveolae-dependent fat uptake
60 have remained obscure.

61 Eps15 homology domain containing protein 2 (EHD2) localizes to the caveolar neck region (6, 21,
62 22). The protein belongs to the dynamin-related EHD ATPase family, which comprises four members in

63 human (EHD1-4), and shows strong expression in human adipose and muscle tissue (human protein atlas)
64 (23). EHD is built of an N-terminal GTPase (G)-domain, which mediates dimerization and oligomerization,
65 a helical domain containing the membrane binding site, and a C-terminal regulatory Eps15 homology (EH)-
66 domain. The proteins exist in a closed auto-inhibited conformation in solution (24). When recruited to
67 membranes, a series of conformational changes aligns the phospholipid binding sites with the membrane
68 and facilitates oligomerization of EHD2 into ring-like structures (25–27).

69 Down-regulation of EHD2 in cell culture results in decreased surface association and increased
70 mobility of caveolae, whereas EHD2 overexpression stabilizes caveolae at the plasma membrane (9, 21,
71 22, 28). This led to the hypothesis that formation of an EHD2-ring at the neck of caveolae restricts caveolar
72 mobility within the membrane. In agreement with this hypothesis, EHD2 assembles in an ATP-dependent
73 fashion into ring-like oligomers *in vitro* and induces the formation of tubular liposomes with an inner
74 diameter of 20 nm, corresponding to the diameter of the caveolar neck (24). Whether EHD2 also controls
75 caveolar membrane dynamics *in vivo* and what the physiological consequences of EHD2 loss at the
76 organismic level are, is unknown.

77 In this study, we found that EHD2 KO mice display enlarged lipid accumulation in white and brown
78 adipose tissue, and increased lipid droplets (LDs) in caveolae-harboring cell types like adipocytes or
79 fibroblasts. In adipose tissue lacking EHD2, caveolae were frequently detached from the plasma
80 membrane and displayed elevated mobility. Furthermore, in two obesity mouse models, as well as in
81 white adipose tissue of obese patients, reduced EHD2 expression and an increased number of detached
82 caveolae were found in visceral fat. Our data establish EHD2 as a negative regulator of caveolae-
83 dependent lipid uptake and implicate a role of caveolar stability and dynamics for lipid homeostasis and
84 obesity.

85

86

87 **Results**

88 **Generation of EHD2 knockout mice**

89 To examine the physiological function of EHD2, a mouse strain with LoxP recognition sites
90 surrounding exon 3 and intron 3 of the *Ehd2* gene was engineered (Fig. 1A). Exon 3 encodes part of the
91 highly conserved GTPase domain (residues 137-167), and its deletion is predicted to result in non-
92 functional protein. Following global removal of exon 3 by crossings with a germ-line specific Cre-deleter
93 strain, offspring mice were back-crossed with the C57BL6/N mouse strain for five generations, yielding a
94 global EHD2 KO mouse model. Genotyping of offspring confirmed the successful deletion of EHD2 exon 3
95 in EHD2 del/del animals (Fig. S1A) and real-time PCR revealed the absence of EHD2 mRNA in the EHD2
96 del/del tissue (Fig. 1B). Western blot analysis indicated the complete loss of EHD2 in WAT and various
97 other tissues of EHD2 del/del mice compared to abundant EHD2 expression in EHD2 +/+ mice (Fig. 1C, Fig.
98 S1B-D). Cav1 and Cavin1 protein levels remained grossly unaltered upon loss of EHD2 (Fig. 1C, Fig. S1D).
99 Accordingly, immunostaining of cryostat sections obtained from EHD2 del/del BAT did not reveal apparent
100 differences in Cav1 or Cavin1 expression and localization (Fig. S1E), whereas EHD2 staining was completely
101 abolished (Fig. 1D).

102

103 **Loss of EHD2 results in increased lipid accumulation**

104 EHD2 del/del mice were born in normal Mendelian ratios, were fertile and did not show any
105 obvious phenotype upon initial inspection. In contrast to the reported loss of white fat mass in Cav1 and
106 Cavin1 KO mouse models (4, 16, 17), one year-old EHD2 del/del male mice were not apparently
107 lipodystrophic and did not display any detectable weight difference when compared to EHD2 del/+ mice
108 (Fig. 1E). However, analysis of the lipid composition in WAT indicated an increased amount of storage
109 lipids (mainly triacylglycerol) in EHD2 del/del mice compared to EHD2 del/+ (Fig. 1F). This suggested that
110 these mice suffered from a more subtle phenotype. Indeed, several of the EHD2 del/del mice showed

111 increased deposits of epigonadal and periinguinal white fat (Fig. 1G) indicating that the storage capacity
112 of normal adipose tissue was dysregulated.

113 When analyzed at the cellular level, white adipocytes of EHD2 del/del mice showed an increased
114 cell size compared to adipocytes from EHD2 del/+ mice or adult C57BL6/N mice (Fig. 1H, Fig. S2A), likely
115 due to increased lipid storage. In contrast to EHD2 del/+ BAT with its distinct brown appearance, EHD2
116 del/del BAT showed increased beige and white coloring (Fig. 1I). Histological inspections of BAT paraffin
117 and cryostat sections stained against the LD coat protein Perilipin1 indicated an increased LD size in EHD2
118 del/del BAT compared to EHD2 del/+ or C57BL6/N mice (Fig. 1J, Fig. S2B-C). As no significant differences
119 lipid accumulation (Fig. S2) were found in EHD2 del/+ and C57BL6/N male mice and to reduce animal
120 numbers, the following experiments were carried out with EHD2 del/+ as control group to EHD2 del/del
121 male mice.

122 Based on the increased lipid accumulation in EHD2-lacking adipocyte tissue, we further
123 investigated if adipocyte differentiation is altered in EHD2 del/del WAT. However, adipogenic marker
124 genes like PPARγ, Retn or Serpina3k displayed no significant expression change in EHD2 del/del WAT
125 compared to EHD2 del/+ WAT (Fig. S2D). The weight adaptation of both genotypes suggested the
126 occurrence of compensatory mechanisms. First, we looked for changes of adiponectin, leptin and insulin
127 plasma levels but did not detect any significant difference in mice lacking EHD2 compared to EHD2 del/+
128 mice (Fig. S3). Free fatty acid concentration in blood plasma was slightly reduced in EHD2 del/del
129 suggesting a possible increase in fatty acid uptake (Fig. S3). Furthermore, we observed a down-regulation
130 of genes involved in *de novo* lipogenesis in isolated WAT obtained EHD2 del/del vs. EHD2 del/+ mice or in
131 primary adipocyte cell cultures (Fig. S5B-D) suggesting that downregulation of lipogenesis is an active
132 mechanism that partially compensates for the increased lipid accumulation.

133

134

135 **Increased lipid droplet size in adipocytes lacking EHD2**

136 To characterize the mechanisms of increased lipid accumulation in EHD2 del/del fat cells, lipid
137 metabolism was investigated in cultured adipocytes. Primary pre-adipocytes were isolated from WAT of
138 EHD2 del/+ and EHD2 del/del mice and differentiated into mature adipocytes, followed by BODIPY
139 staining to measure LD sizes. Undifferentiated EHD2 del/del pre-adipocytes showed increased LD size, a
140 difference that was even more pronounced in differentiated EHD2 del/del adipocytes compared to EHD2
141 del/+ (Fig. 2A-B). 3D reconstruction of EHD2 del/del differentiated adipocytes illustrates an extensively
142 increased volume of some LDs (Fig. 2C).

143 We addressed the possibility that increased lipid uptake is a secondary effect of EHD2 deletion
144 mediated via putative organ cross-talk. We therefore repeated the experiments with cultivated
145 adipocytes derived from EHD2 cKO flox/flox mice, in which EHD2 expression was down-regulated by
146 expression of Cre recombinase via viral transfection (AAV8). Again, EHD2 removal led to increased LD
147 growth (Fig. 2D-E), indicating a cell-autonomous function of EHD2 in controlling lipid uptake.

148 LD growth is mainly mediated by extracellular fatty acid uptake and conversion into triglycerides,
149 whereas increased glucose uptake and *de novo* lipogenesis play minor roles in this process (29, 30). Fatty
150 acids and lipids are present at high concentrations in fetal bovine serum (FBS). Addition of delipidated FBS
151 during adipocyte differentiation resulted in complete loss of LD in both genotypes (Fig. S4A), whereas
152 glucose-depletion led to a general impairment of adipocyte differentiation. Importantly, enlarged LDs
153 were still observed in KO adipocytes even under conditions of glucose depletion (Fig. S4A). These data led
154 us to hypothesize that the increased LD size in EHD2 del/del adipocytes may be a consequence of
155 increased fatty acid uptake, in line with the suggested function of caveolae in fatty acid uptake (31–33).

156 To test this possibility directly, we monitored the uptake of extracellularly added fatty acids into
157 differentiated adipocytes using BODIPY-labelled dodecanoic acid (FA12) paired with FACS analysis. After
158 5 min, only a minor fraction of EHD2 del/+ adipocytes displayed intense BODIPY staining (R2, for definition

159 see Fig. 2F). This R2 population increased to more than 30% after 60 min of FA12 treatment. EHD2 del/del
160 adipocytes displayed increased BODIPY staining at both early and late time points (Fig. 2F-H; Fig. S4B-D),
161 indicating accelerated lipid uptake. This conclusion was further supported by light microscopy imaging,
162 which revealed more intense BODIPY staining of EHD2 del/del cells compared to EHD2 del/+ adipocytes
163 after 60 min of fatty acid incubation (Fig. 2G). In contrast, EHD2 del/+ and EHD2 del/del adipocytes did
164 not differ with respect to their ability to take up extracellularly added glucose (Fig. S4E-G). Previously, an
165 involvement of EHD2 in the autophagic engulfment of LDs (lipophagy) was suggested (34). However,
166 inducing starvation by incubation of differentiated adipocytes with Hank's balanced salt solution (HBSS)
167 revealed no differences in the release of stored lipids in EHD2 del/+ and EHD2 del/del adipocytes, and
168 both genotypes displayed similar reductions in lipid accumulation (Fig. S5A). These data indicate that loss
169 of EHD2 does not affect the release of fatty acids or lipophagy, but specifically controls LD size by
170 regulating fatty acid uptake.
171
172 **Loss of EHD2 results in detachment of caveolae from the plasma membrane *in vivo***
173 Given the known role of caveolae in the uptake of fatty acids (16), we hypothesized that EHD2
174 may restrict fatty acid uptake by controlling caveolar function and/ or dynamics. To test whether loss of
175 EHD2 affects caveolar morphology, WAT and BAT were analyzed by electron microscopy (EM). Caveolae
176 in EHD2 del/+ BAT were mostly membrane-bound and displayed the characteristic flask-shaped
177 morphology (Fig. 3A, white arrows, ratio detached/membrane bound caveolae = 0.27). Strikingly, an
178 increased number of caveolae appeared detached from the plasma membrane in BAT isolated from EHD2
179 del/del mice compared to EHD2 del/+ controls, as judged from the complete closure of the lipid bilayer in
180 the plasma membrane and the caveolae (Fig. 3A, B, black arrows, ratio detached/membrane bound
181 caveolae = 1.75). The total number of caveolae, as well as the caveolar diameter and size, were unchanged
182 in brown adipocytes lacking EHD2.

183 An increased number of detached caveolae were also observed in EHD2 del/del white adipocytes
184 compared to EHD2 del/+ cells from littermate controls (Fig. 3C, D, black and white arrow heads, ratio
185 detached/membrane bound caveolae (del/del) = 1.2 vs. ratio (del/+) = 0.24). In white adipocytes, the total
186 number of caveolae was reduced, while both caveolar size and diameter were increased in EHD2 del/del
187 compared to EHD2 del/+ animals (Fig. 3D). Cav1 immunogold labeling confirmed that the round vesicles
188 close the plasma membrane, indeed, were detached caveolae (Fig. 3E). 3D visualization of EHD2 del/del
189 brown adipocyte by electron tomography (ET) further indicated that the majority of detached caveolae in
190 2D EM images were not connected to the plasma membrane (Fig. 3F, G, Movie S1) but localized 20-30 nm
191 underneath (Fig. 3G a, b), although some caveolae close to the plasma membrane showed thin
192 connections (Fig. 3G b, d, white arrow head). Taken together, EM and ET reveal an increased detachment
193 of caveolae from the plasma membrane in EHD2 del/del adipocytes, suggesting a crucial function for EHD2
194 in the stabilization of caveolae at the plasma membrane.
195
196 **Increased caveolar mobility in EHD2 knockout cells**
197 To further dissect the interplay of caveolar mobility and LD growth at the molecular level, we
198 investigated caveolar mobility and endocytosis in mouse embryonic fibroblasts (MEFs) by total internal
199 reflection fluorescence (TIRF) microscopy. MEFs derived from EHD2 +/+ and del/del mice were transfected
200 with pCav1-EGFP to label single caveolae. As illustrated in Fig. 4A, regions of moderate Cav1 expression
201 were investigated to ensure that distinct Cav1 spots were observed during the analysis. Live TIRF imaging
202 of EHD2 +/+ MEFs showed a slow or no continuous movement for the majority of investigated caveolae
203 (Movie S2). However, single caveolae moved along the plasma membrane or left the TIRF illumination
204 zone towards the inside of the cell, indicative of their spontaneous detachment, as previously reported
205 (21). Strikingly, movement and velocity of caveolae was greatly increased in EHD2 del/del MEFs (Movie
206 S3), not allowing Cav1 single spots to be tracked. Line scan analysis revealed a greatly reduced number of

207 fixed, non-moving Cav1 spots (referred to as lines in Fig. 4B) in EHD2 del/del MEFs compared to EHD2 +/+
208 cells. Moreover, a larger number of highly mobile Cav1 sparks, reflecting fast moving caveolae, was found
209 in EHD2 del/del cells (Fig. 4A, B). Re-expression of EHD2 in EHD2 del/del MEFs reduced the mobility of
210 caveolae, often leading to their immobilization (Fig. S6, Movie S4).
211
212 **Determinants of EHD2-mediated fatty acid uptake**
213 We further characterized the determinants of the observed lipid uptake in MEFs. Similar to EHD2
214 del/del adipocytes, EHD2 del/del MEFs showed increased lipid accumulation and LD size after adipogenic
215 differentiation, as illustrated by Oil red O staining (Fig. S7A) and BODIPY staining (Fig. S7B, C).
216 Furthermore, both storage and membrane lipids were increased in MEFs lacking EHD2 (Fig. S7D). Re-
217 expression of an EGFP-tagged EHD2 version in in EHD2 +/+ and del/del MEFs rescued the observed LD
218 phenotype, even reducing the size of LDs compared to EGFP expressing cells (Fig. 5A, B). These data
219 indicate a general and cell autonomous role of EHD2 in the control of LD growth and size that is not
220 restricted to fat cells.
221 To identify the functional regions within EHD2 that are crucial for regulating lipid uptake, we
222 transfected EHD2 del/del MEFs with various EGFP-tagged EHD2 deletion constructs. EHD2 constructs
223 lacking the N-terminus, the EH-domain or both, rescued EHD2 loss, resulting in smaller LDs (Fig. 5C, S7E).
224 In contrast, expression of single EHD2 mutants affecting membrane binding (F322A) or
225 oligomerization/ATPase activity of EHD2 (F122A) did not reduce LD size, indicating a crucial role of these
226 properties for EHD2 function.
227 To analyze if the observed phenotype in EHD2 del/del MEFs was dependent on caveolae, MEFs
228 lacking EHD2 were treated with Cav1 siRNA to eliminate caveolae. LD size in EHD2 del/del MEFs was
229 significantly decreased following depletion of Cav1 (Fig. 5D, E), indicating that the effects of EHD2 on LD
230 size require and likely are mediated by caveolae.

231 It was previously reported that dynamin is located on caveolae (35). Consistent with a role of
232 dynamin in caveolae function, overexpression of a dynamin 2 dominant negative mutant (pGFP-Dyn2-
233 K44A, Fig. 5F, G) completely abolished the size increase of LDs in EHD2 del/del MEFs, suggesting a role for
234 dynamin in fatty acid uptake via caveolae.

235 Previous work has implicated the fatty acid binding membrane protein CD36 in caveolae-
236 dependent fatty acid uptake (31, 36, 37). To probe a possible function of CD36 in EHD2-dependent lipid
237 uptake, CD36 expression in MEFs was downregulated by treatment with either one of three specific CD36
238 siRNA. Antibody staining confirmed the efficient knockdown of CD36 in EHD2 +/+ and del/del MEFs (Fig.
239 5H). Removal of CD36 in EHD2 +/+ and del/del MEFs dramatically decreased the size of LDs compared to
240 a control siRNA treated cells (Fig. 5H). Hence, the observed enlargement of LDs in cells lacking EHD2
241 depends on CD36. These converging lines of evidence suggest that caveolae dynamics is key to the
242 regulation of fatty acid internalization and that this is coupled to the previously shown importance of
243 CD36 and caveolin as fatty acid binding proteins.

244

245 **Decreased EHD2 expression in genetic obesity models or in diet induced obesity**

246 Our data indicate an EHD2-dependent regulation of lipid uptake in adipose tissue. If this were of
247 physiological relevance, one might expect EHD2 expression to be dysregulated in obese mice and men.
248 We therefore investigated if EHD2 expression is altered in two obesity-related mouse models, ob/ob and
249 NZO (38). Indeed, WAT obtained from ob/ob and NZO mice showed reduced EHD2 expression compared
250 to C57BL6/N mice fed by standard diet (Fig. 6A). When investigating adipocytes from ob/ob mice, a higher
251 proportion of detached caveolae were found in the obesity mouse model (ratio detached/membrane
252 bound caveolae = 1.4 vs. 0.35 in C57BL6/N mice fed with standard diet, Fig. 6B, C). In addition, we analyzed
253 EHD2 expression in visceral and subcutaneous WAT from patients ranking in their body mass index (BMI)
254 from normal to morbid obesity (BMI<25 – BMI >40, Fig. 6D, E). In both depots, EHD2 expression was

255 highest in normal weight subjects and was significantly lower in overweight and obese people, whereas
256 EHD2 expression did not differ between different obesity stages. These data imply that EHD2 expression
257 is regulated by lipid uptake and load and suggest that EHD2-mediated caveolar dynamics may be altered
258 in obesity.
259
260 **Discussion**
261 Here, we identify EHD2 as a negative regulator of caveolae-dependent lipid uptake. Loss of EHD2
262 resulted in increased lipid accumulation, which was observed in adipose tissue of the whole organism as
263 well as in cell culture-based experiments. Loss of EHD2 was associated with the detachment of caveolae
264 from the plasma membrane, higher caveolar mobility and increased lipid uptake. We demonstrate that
265 caveolae, dynamin 2 and the fatty acid translocase CD36 play a role in the EHD2-dependent lipid uptake
266 pathway. In addition, obese mouse models exhibit decreased EHD2 expression in WAT and in addition,
267 also obese patients showed a reduction in EHD2 gene expression. Thus, our study reveals a cell-
268 autonomous caveolae dependent lipid uptake route that is controlled by EHD2 and modified by metabolic
269 conditions.
270 For some time, caveolae have been implicated in lipid uptake. Thus, mice lacking caveolae showed
271 reduced fat mass and did not develop any form of obesity. In addition, Pohl et al. (39) observed decreased
272 oleate uptake after expression of a dominant-negative Cav1 mutant. The EHD2 KO mouse model,
273 described here, revealed the opposite phenotype, e.g. a caveolae gain-of-function *in vivo* model. In EHD2
274 KO mice, caveolae were more often detached from the plasma membrane and showed a higher mobility
275 and faster lipid uptake, resulting in enlarged LDs. Unlike in Cav1 over-expressing mice (19), which also
276 show increased fatty acid uptake, the number of caveolae was not increased in EHD2 KO mice. This
277 supports a model in which not only caveolae number, but also caveolar dynamics play a crucial role in this
278 process (Fig. 6F). Furthermore, such idea is in line with our structural findings that EHD2 can form ring-

279 like oligomers that may stabilize the neck of caveolae (24–27), thereby restricting caveolar mobility (21,
280 22). Based on studies in EHD2 KO NIH 3T3 cell line, Yeow et al. (40) suggested that EHD1 and/or EHD4
281 could rescue loss of EHD2 during its role in membrane protection. However, we did not find rescue of
282 caveolae detachment and lipid uptake in EHD2 KO cells by other EHD family members.

283 The detailed pathway of caveolae-dependent cellular lipid uptake has been intensively studied (4,
284 20, 31, 32, 41), but the exact molecular mechanisms are still unclear. Our observation indicate that fatty
285 acid uptake depends on caveolar dynamics, detachment and most likely caveolae endocytosis and is
286 regulated by EHD2. However, it remains elusive how caveolar shuttling is linked to the growth of lipid
287 droplets. The EHD2 knockout model may be a useful tool to further dissect the molecular lipid uptake
288 mechanism.

289 The loss of EHD2 on the cellular level led to increased fat deposits on the organismic level, which
290 was particularly evident in older animals. The observed phenotype based on the global loss of EHD2 could
291 be influenced by organ-organ interactions (42). However, we did not find any evidence for differences in
292 adipocyte derived secretory factors, such as leptin (Fig. S3). Furthermore, increased lipid uptake was
293 dependent on caveolae, as shown by Cav1 knockdown experiments, and lipid droplet growth could
294 specifically be induced by viral transfection of Cre recombinase in EHD2 cKO flox/flox, but not in flox/wt
295 adipocytes. Thus, increased lipid uptake is caused by a cell-autonomous, caveolae-dependent mechanism.
296 As the WAT distribution and lipid accumulation is known to differ in male and female mice, further studies
297 are required to analyze potential sex-specific differences in EHD2-dependent lipid uptake.

298 Despite the observed lipid accumulation in mice lacking EHD2, the body weight of EHD2 del/del
299 and EHD2 del/+ mice was unaltered, suggesting metabolic compensation. In line with this idea, EHD2
300 del/del WAT and cultivated EHD2 del/del adipocytes showed a significant reduction in expression levels
301 of genes involved in *de novo* lipogenesis like SREBP1 or FAS indicating a strong downregulation of glucose-
302 dependent fatty acid production in fat cells. Similar compensatory mechanisms were noted in patients

303 suffering from obesity (43–45). Remarkably, the expression levels of EHD2 in WAT from obese patients as
304 well as in WAT of two obese mouse models (ob/ob and NZO mice) and of EHD2 del/+ mice treated with a
305 long-term high fat diet were significantly reduced. Thus, expression of EHD2 appears to negatively
306 correlate with adipocyte size, therefore reflecting the situation in the EHD2 KO mouse (see also (46)). We
307 speculate that an imbalance in number, life-time and mobility of caveolae may accompany and possibly
308 actively contribute to the development and progression of obesity. Accordingly, pharmacological
309 approaches to enhance EHD2 expression or its stabilization at the plasma membrane could reduce lipid
310 uptake and consequently help to treat obesity in patients.

311 In conclusion, our study reveals that EHD2 controls a caveolae-dependent cellular lipid uptake
312 pathway.

313

314 **Methods**

315 Please see SI for detailed description of all methods and material.

316 **EHD2 delta E3 mouse strain generation.** The EHD2 targeting construct was generated by insertion of two
317 lox P sequences flanking exon 3 of EHD2 genomic DNA by homologous recombination in *E.coli* as
318 previously described (47) including a pGK Neomycin and a diphtheria toxin A (DTA) cassette.
319 Electroporation of the linearized targeting vector in R1 ES cells was performed. Mice carrying a loxP-
320 flanked Exon 3 of EHD2 gene were mated to Cre deleter mice to generate EHD2 mutant (del/del) mice.
321 After backcrossing the EHD2 del/del mice with C57BL6/N (Charles River, between 20-30 weeks, male) for
322 6 generations only male EHD2 del/del or EHD2 del/+ (as control) mice were used and littermates were
323 randomly assigned to experimental groups. All animals were handled accordingly to governmental animal
324 welfare guidelines and were housed under standard conditions.

325 **Obesity Mouse Models.** Male NZO/HIBomDife (German Institute of Human Nutrition, Nuthetal,
326 Germany), C57BL/6J (Charles River Laboratories, Sulzfeld, Germany) and B6.V-Lepob/ob/JBomTac (B6-
327 ob/ob) mice (Charles River Laboratories, Calco, Italy) were housed under standard conditions
328 (conventional germ status, 22 °C with 12 hour /dark cycling). NZO and C57BL/6J mice were fed were fed
329 standard chow diet (Ssniff, Soest). Starting at 5 weeks of age B6-ob/ob received carbohydrate free diet
330 (48). Mice were sacrificed at an age of 20-22 weeks.

331 **Oil Red O staining.** LDs in tissue sections or cultivated adipocytes and MEFs were stained with Oil Red O
332 as published by (49).
333 **Human EHD2 expression.** All participants were recruited by University Leipzig (approval numbers: 265-
334 08, 159-12-21052012, and 017-12-23012012) and samples were treated as previously described (50).
335 **Immunocytostaining and LD staining of cultivated cells.** Adipocytes or MEFs were seeded on fibronectin
336 (Sigma) coated glass dishes (ThermoFisher). Cells were washed with PBS, treated with 4% PFA for 10 min
337 and blocking buffer (1%donkey serum/1% TritonX100/PBS) for 20 min. The first antibody was incubated
338 for 1 h, followed by secondary antibody and DAPI stain. For LD staining, BODIPY (Invitrogen, saturated
339 solution) or Nile Red (Sigma, saturated solution) was diluted to 1:1000 in PBS and applied for 30 min. The
340 stained cells were washed and the glass dishes were placed on conventional microscope slides and
341 embedded in ImmoMount. Zeiss LSM700 or Zeiss LSM880 microscopes and ImageJ/Fij were used.
342 **Transmission Electron microscopy (TEM).** Mice were fixed by perfusion with 4% (w/v) formaldehyde in
343 0.1 M phosphate buffer. Tissue blocs were postfixed in phosphate buffered 2.5% (v/v) glutaraldehyde,
344 treated with 1% (v/v) osmium tetroxide, dehydrated in a graded series of ethanol and embedded in the
345 PolyBed® 812 resin (Polysciences Europe GmbH). Ultrathin sections (60-80 nm) were cut (Leica
346 microsystems) and stained with uranyl acetate and lead citrate before image acquisition. Samples were
347 examined at 80 kV with a Zeiss EM 910 electron microscope. Acquisition was done with a Quemesa CDD
348 camera and the iTEM software (Emsis GmbH).
349 **Electron tomography (ET).** To obtain electron tomograms 250 nm slices of EHD2 del/del BAT were
350 prepared of samples embedded in resin and treated as described for TEM. The samples were tilted from
351 60 to -60° in 2° steps and examined at 120 kV with a FEI Talos electron microscope. FEI tomography
352 software was used for acquisition of tomograms, detailed analysis and reconstruction was done with
353 Inspect3D, Amira (both obtained from FEI) and IMOD (University of Colorado, USA).
354 **Fatty acid uptake assay.** EHD2 del/+ and EHD2 del/del pre-adipocytes were seeded in 6-well plates
355 (100.000 cells/well) and differentiated in mature adipocytes as described above. The fatty acid uptake
356 assay was performed as described elsewhere (51). Briefly, differentiated adipocytes were starved for 1 h
357 with serum-free DMEM. Next, 2 µM dodecanoic acid (FA12) labelled with BODIPY (Molecular probes
358 #D3822) diluted in serum-free DMEM + 10 µg/ml insulin was added to the adipocytes and incubated for
359 5-60 min at 37°C followed by FACS. Glucose uptake was measured with 200 µM 2-NBDG (2-deoxy-2-[(7-
360 nitro-2,1,3-benzoxadiazol-4-yl)amino]-D-glucose, molecular probes #N13195) diluted in serum-free
361 DMEM + 10 µg/ml insulin.
362

Acknowledgments

We thank Petra Stallerow for taking care of the EHD2 delta E3 mouse strain, Karin Jacobi for advice with the animal application, Vivian Schulz and Carola Bernert for helping with the genotyping of the mice, Claudio Shah for purifying the EHD2 antiserum, and the advanced light imaging facility at MDC for technical support. The authors acknowledge financial support from the Deutsche Forschungsgemeinschaft (DFG; SFB 958/A7 to V.H., A12 to O.D., A13 to A.S.) and support by The Initiative and Networking Fund of the Helmholtz Association.

Author Contributions

C.M. planned, performed and analyzed all experiments if not otherwise indicated. C.M. and O.D. wrote the manuscript, with input from all authors. S.K. performed and analyzed all EM imaging, C.M. analyzed EM images, S.K. and C.M. performed and analyzed ET. I.L. generated the EHD2 KO mouse model and performed in situ hybridization. W.J. analyzed blood plasma markers and EHD2 expression in obesity mouse models. M.L. helped during TIRF imaging and discussed experiments, A.M. isolated primary MEF and performed the EHD2 Western Blot. E.L. performed lipid droplet staining experiments after Cav1 knockdown. M.K. and M.B. recruited obese patients and handled human samples. A.S., V.H., R.L., C.B. and D.N.M. discussed potential experiments and the manuscript. O.D. wrote the mouse animal application with help of D.N.M. and C.M.

Declaration of Interests

The authors declare no competing interests.

References

1. Cheng JPX, Nichols BJ (2016) Caveolae : One Function or Many ? *Trends Cell Biol* 26(3):177–189.
2. Sinha B, et al. (2011) Cells respond to mechanical stress by rapid disassembly of caveolae. *Cell* 144(3):402–413.
3. Torrino S, et al. (2018) EHD2 is a mechanotransducer connecting caveolae dynamics with gene transcription. 1–14.
4. Liu L, et al. (2008) Deletion of Cavin/PTRF Causes Global Loss of Caveolae, Dyslipidemia, and Glucose Intolerance. *Cell Metab* 8(4):310–317.
5. Ju H, Zou R, Venema VJ, Venema RC (1997) Direct Interaction of Endothelial Nitric-oxide Synthase

394 and Caveolin-1 Inhibits Synthase Activity. *J Biol Chem* 272(30):18522–18525.

395 6. Ludwig A, et al. (2013) Molecular Composition and Ultrastructure of the Caveolar Coat Complex.
396 *PLoS Biol* 11(8). doi:10.1371/journal.pbio.1001640.

397 7. Ludwig A, Nichols BJ, Sandin S (2016) Architecture of the caveolar coat complex. *J Cell Sci*:3077–
398 3083.

399 8. Stoeber M, et al. (2016) Model for the architecture of caveolae based on a flexible, net-like
400 assembly of Cavin1 and Caveolin discs. *Proc Natl Acad Sci U S A*:201616838.

401 9. Mohan J, Moren B, Larsson E, Holst MR, Lundmark R (2015) Cavin3 interacts with cavin1 and
402 caveolin1 to increase surface dynamics of caveolae. *J Cell Sci* 128(5):979–991.

403 10. Kovtun O, Tillu VA, Ariotti N, Parton RG, Collins BM (2015) Cavin family proteins and the assembly
404 of caveolae. *J Cell Sci* 128(7):1269–1278.

405 11. Hansen CG, Howard G, Nichols BJ (2011) Pacsin 2 is recruited to caveolae and functions in
406 caveolar biogenesis. *J Cell Sci* 124(Pt 16):2777–2785.

407 12. Senju Y, Itoh Y, Takano K, Hamada S, Suetsugu S (2011) Essential role of PACSIN2/syndapin-II in
408 caveolae membrane sculpting. *J Cell Sci* 124(12):2032–2040.

409 13. Seemann E, et al. (2017) Deciphering caveolar functions by syndapin III KO-mediated impairment
410 of caveolar invagination. *Elife* 6:1–37.

411 14. Drab M, et al. (2001) Loss of caveolae, vascular dysfunction, and pulmonary defects in caveolin-1
412 gene-disrupted mice. *Science (80-)* 293(5539):2449–2452.

413 15. Hill MM, et al. (2008) PTRF-Cavin, a Conserved Cytoplasmic Protein Required for Caveola
414 Formation and Function. *Cell* 132(1):113–124.

415 16. Razani B, et al. (2002) Caveolin-1-deficient mice are lean, resistant to diet-induced obesity, and
416 show hypertriglyceridemia with adipocyte abnormalities. *J Biol Chem* 277(10):8635–8647.

417 17. Martin S, et al. (2012) Caveolin-1 Deficiency Leads to Increased Susceptibility to Cell Death and
418 Fibrosis in White Adipose Tissue: Characterization of a Lipodystrophic Model. *PLoS One* 7(9):1–9.

419 18. Ding SY, et al. (2014) Pleiotropic effects of cavin-1 deficiency on lipid metabolism. *J Biol Chem*
420 289(12):8473–8483.

421 19. Briand N, et al. (2014) Caveolin-1 expression and cavin stability regulate caveolae dynamics in
422 adipocyte lipid store fluctuation. *Diabetes* 63(12):4032–4044.

423 20. Pohl J, et al. (2004) Long-Chain Fatty Acid Uptake into Adipocytes Depends on Lipid Raft Function.
424 *Biochemistry* 43(14):4179–4187.

425 21. Morén B, et al. (2012) EHD2 regulates caveolar dynamics via ATP-driven targeting and
426 oligomerization. *Mol Biol Cell* 23(7):1316–29.

427 22. Stoeber M, et al. (2012) Oligomers of the ATPase EHD2 confine caveolae to the plasma
428 membrane through association with actin. *EMBO J* 31(10):2350–2364.

429 23. Uhlén M, et al. (2015) Tissue-based map of the human proteome. 347(6220).
430 doi:10.1126/science.1260419.

431 24. Daumke O, et al. (2007) Architectural and mechanistic insights into an EHD ATPase involved in
432 membrane remodelling. *Nature* 449(7164):923–7.

433 25. Shah C, et al. (2014) Structural insights into membrane interaction and caveolar targeting of
434 dynamin-like EHD2. *Structure* 22(3):409–420.

435 26. Hoernke M, et al. (2017) EHD2 restrains dynamics of caveolae by an ATP-dependent, membrane-
436 bound, open conformation. *Proc Natl Acad Sci U S A* 114(22):E4360–E4369.

437 27. Melo AA, et al. (2017) Structural insights into the activation mechanism of dynamin-like EHD
438 ATPases. *Proc Natl Acad Sci* 114(22):5629–5634.

439 28. Shvets E, Bitsikas V, Howard G, Hansen CG, Nichols BJ (2015) Dynamic caveolae exclude bulk
440 membrane proteins and are required for sorting of excess glycosphingolipids. *Nat Commun*
441 6:6867–6883.

442 29. Rutkowski JM, Stern JH, Scherer PE (2015) The cell biology of fat expansion. *J Cell Biol*
443 208(5):501–512.

444 30. Wilfling F, et al. (2013) Triacylglycerol synthesis enzymes mediate lipid droplet growth by
445 relocalizing from the ER to lipid droplets. *Dev Cell* 24(4):384–399.

446 31. Ring A, Le Lay S, Pohl J, Verkade P, Stremmel W (2006) Caveolin-1 is required for fatty acid
447 translocase (FAT/CD36) localization and function at the plasma membrane of mouse embryonic
448 fibroblasts. *Biochim Biophys Acta - Mol Cell Biol Lipids* 1761(4):416–423.

449 32. Pohl J (2002) Uptake of long-chain fatty acids in HepG2 cells involves caveolae: analysis of a novel
450 pathway. *J Lipid Res* 43(9):1390–1399.

451 33. Pilch PF, Meshulam T, Ding S, Liu L (2011) Caveolae and lipid trafficking in adipocytes. *Clin Lipidol*
452 6(1):49–58.

453 34. Li Z, et al. (2016) A novel Rab10-EHBP1-EHD2 complex essential for the autophagic engulfment of
454 lipid droplets. *Sci Adv* 2(12):1–16.

455 35. Oh P, McIntosh DP, Schnitzer JE (1998) Dynamin at the neck of caveolae mediates their budding
456 to form transport vesicles by GTP-driven fission from the plasma membrane of endothelium. *J*
457 *Cell Biol* 141(1):101–114.

458 36. Eyre NS, Cleland LG, Tandon NN, Mayrhofer G (2007) Importance of the carboxyl terminus of
459 FAT/CD36 for plasma membrane localization and function in long-chain fatty acid uptake. *J Lipid*
460 *Res* 48(3):528–542.

461 37. Aboulaich N, Vainonen JP, Stralfors P, Vener A V (2004) Vectorial proteomics reveal targeting,
462 phosphorylation and specific fragmentation of polymerase I and transcript release factor (PTRF)
463 at the surface of caveolae in human adipocytes. *Biochem J* 383(Pt 2):237–48.

464 38. Kleinert M, et al. (2018) Animal models of obesity and diabetes mellitus. *Nat Rev Endocrinol*
465 14(3):140–162.

466 39. Pohl J, Axel R, Korkmaz U, Ehehalt R, Stremmel W (2005) FAT/CD36-mediated Long-Chain Fatty
467 Acid Uptake in Adipocytes Requires Plasma Membrane Rafts. *Mol Biol Cell* 16(1):24–31.

468 40. Yeow I, et al. (2017) Article EHD Proteins Cooperate to Generate Caveolar Clusters and to
469 Maintain Caveolae during Repeated Article EHD Proteins Cooperate to Generate Caveolar
470 Clusters and to Maintain Caveolae during Repeated Mechanical Stress. *Curr Biol* 27:1–12.

471 41. Briand N, et al. (2014) Caveolin-1 expression and cavin stability regulate caveolae dynamics in
472 adipocyte lipid store fluctuation. *Diabetes* 63(12):4032–4044.

473 42. Stern JH, Rutkowski JM, Scherer PE (2016) Review Adiponectin , Leptin , and Fatty Acids in the
474 Maintenance of Metabolic Homeostasis through Adipose Tissue Crosstalk. *Cell Metab* 23(5):770–
475 784.

476 43. Guiu-Jurado E, et al. (2015) Downregulation of de novo fatty acid synthesis in subcutaneous
477 adipose tissue of moderately obesewomen. *Int J Mol Sci* 16(12):29911–29922.

478 44. Eissing L, et al. (2013) De novo lipogenesis in human fat and liver is linked to ChREBP- β and
479 metabolic health. *Nat Commun* 4:1528–1539.

480 45. Solinas G, Borén J, Dulloo AG (2015) De novo lipogenesis in metabolic homeostasis: More friend
481 than foe? *Mol Metab* 4(5):367–377.

482 46. Sonne SB, et al. (2017) Obesity is associated with depot-specific alterations in adipocyte DNA
483 methylation and gene expression. *Adipocyte* (May):1–10.

484 47. Liu P, et al. (2003) A Highly Efficient Recombineering-Based Method for Generating Conditional
485 Knockout Mutations. *Genome Res* 13:476–484.

486 48. Kluth O, et al. (2015) Identification of Four Mouse Diabetes Candidate Genes Altering β-Cell
487 Proliferation. *PLOS Genet* 11(9):e1005506.

488 49. Mehlem A, Hagberg CE, Muhl L, Eriksson U, Falkevall A (2013) Imaging of neutral lipids by oil red
489 O for analyzing the metabolic status in health and disease. *Nat Protoc* 8(6):1149–1154.

490 50. Guiu-jurado E, et al. (2016) Bone Morphogenetic Protein 2 (BMP2) may Contribute to Partition
491 of Energy Storage into Visceral and Subcutaneous Fat Depots. *Obesity* 24(10):2092–2100.

492 51. Dubikovskaya E, Chudnovskiy R, Karateev G, Park HM, Stahl A (2014) Measurement of long-chain
493 fatty acid uptake into adipocytes. *Methods Enzym* 538(1):107–134.

494

495 **Figures**

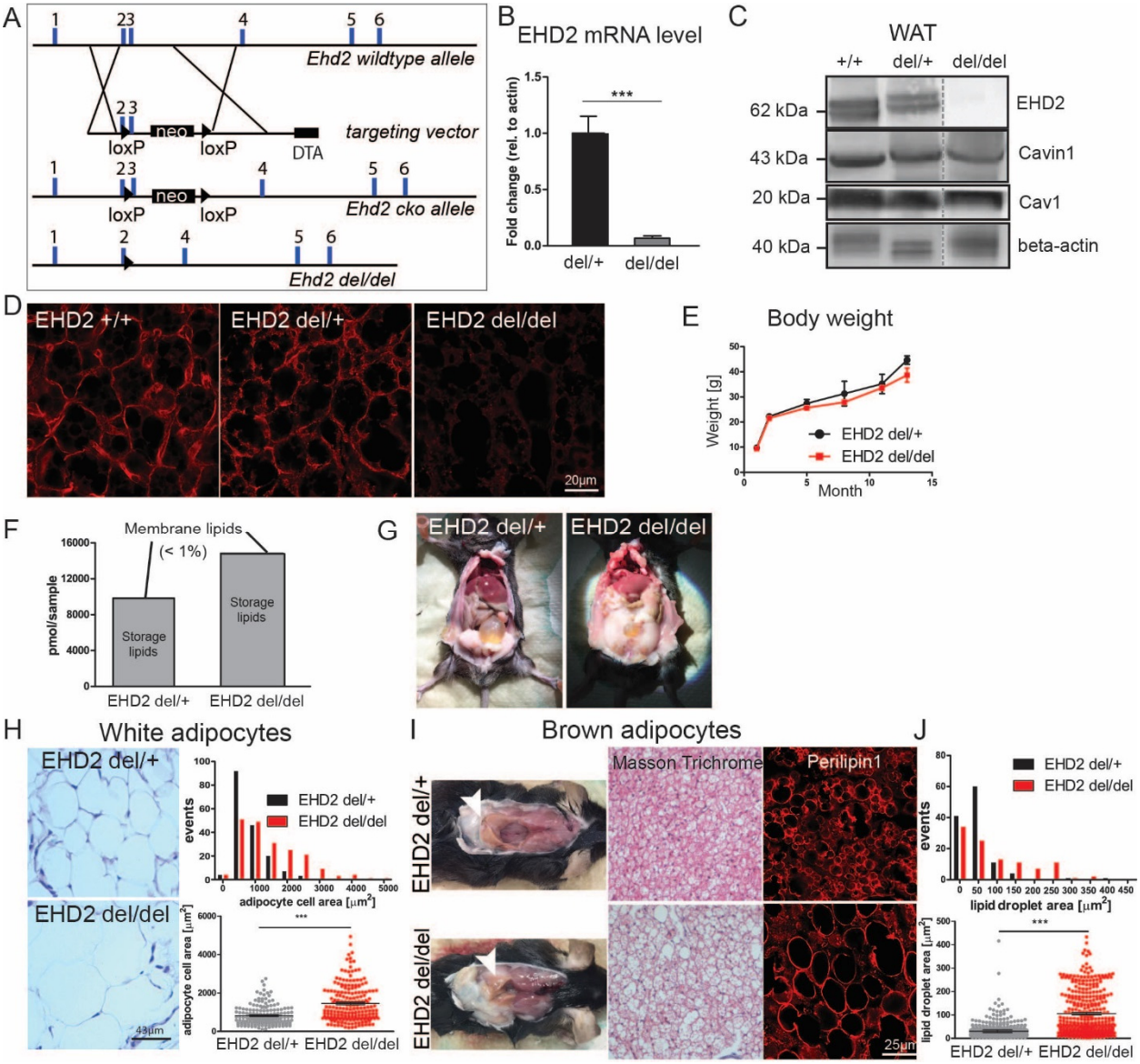

496

497 **Fig.1 Loss of EHD2 results in increased lipid accumulation in white and brown adipose tissue**

498 **A** Generation of the EHD2 KO mouse model. A targeting vector containing a pGK-Neomycin (neo) cassette
499 and loxP sites flanking exon 3 was placed in the EHD2 wt allele. EHD2 del/del mice were obtained by
500 breeding with Cre-deleter mouse strain (DTA - diphtheria toxin A).

501 **B** EHD2 mRNA level in EHD2 del/+ and EHD2 del/del mice (mRNA from BAT, n = 5).

502 **C** Western Blot analysis of WAT of EHD2+/+, +/- and -/- mice against EHD2, Cav1 and Cavin1.

503 **D** EHD2 immuno-staining in BAT cryostat sections from EHD2 +/+, del/+ and del/del mice.

504 **E** The body weight was monitored over 12 months (n = 7).

505 **F** Lipid composition analysis of 15 µg WAT obtained from EHD2 del/+ or EHD2 del/del mice.

506 **G** EHD2 del/+ and EHD2 del/del mice during preparation.

507 **H** Masson Trichrome staining of WAT paraffin sections of EHD2 del/+ and EHD2 del/del. Detailed analysis
508 of the adipocytes cell size (K, n(del/+) = 172/3, n(del/del) = 199/3).
509 **I** EHD2 del/del mice showed decreased BAT in the neck region. Instead, WAT was integrated into the BAT
510 depots.
511 **J** Masson Trichrome staining of EHD2 del/del BAT paraffin sections and BAT cryostat sections stained
512 against the LD coat protein Perilipin1. LD size was measured in BAT cryostat sections (M, n(del/+) = 118/3,
513 n(del/del) = 104/3).
514 Line graph represents mean +/- SE, column bar graphs show mean + SE, normal distributed groups were
515 analyzed by t-test, not normally distributed values with Mann Withney U test, * $P<0.05$, *** $P<0.0001$.
516 For comparison to C57BL6/N, see also Fig. S1-S3.
517
518

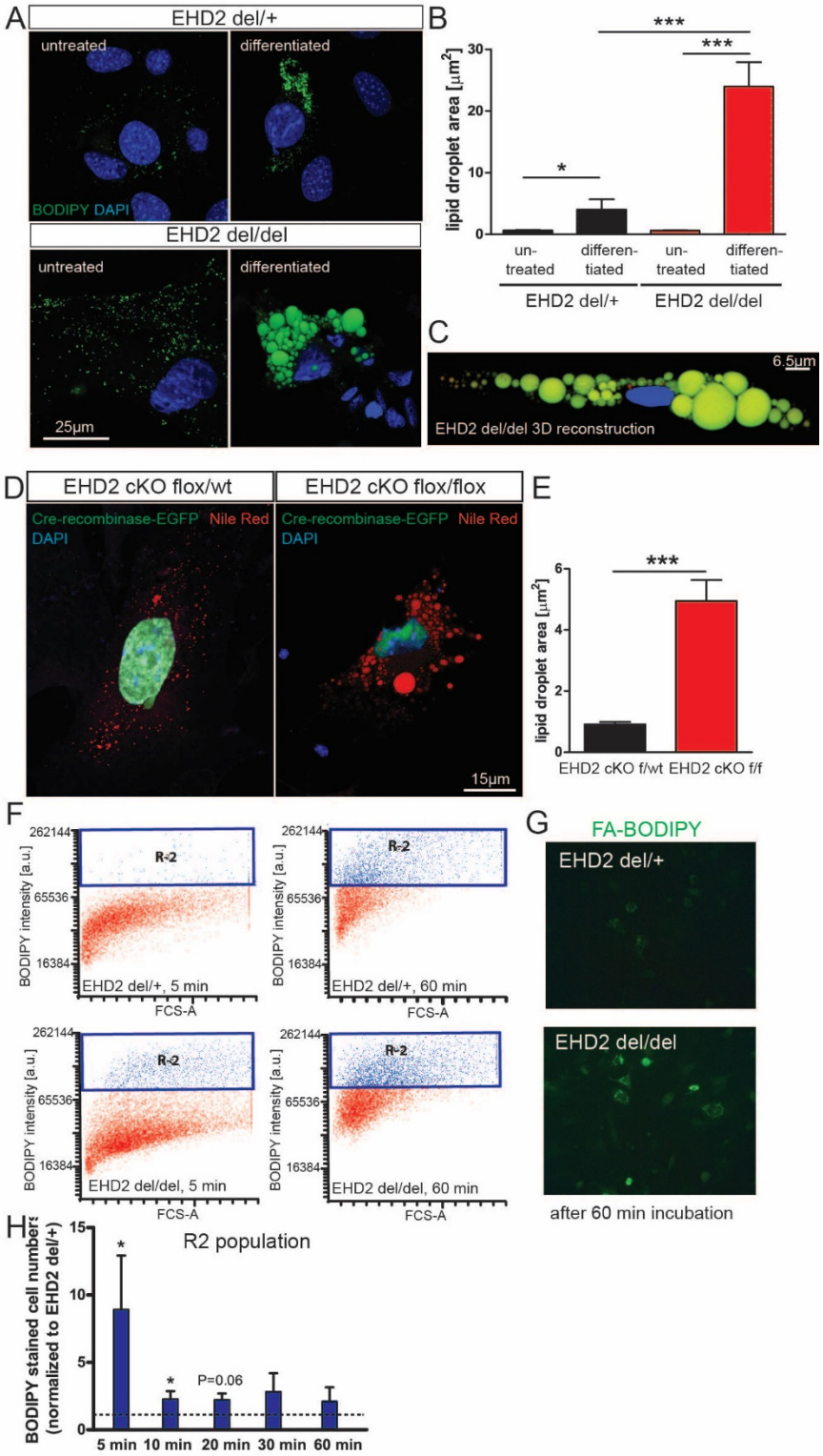

Fig. 2: EHD2 del/del adipocytes show faster fatty acid uptake

521 **A-C** Analysis of LD size in EHD2 del/del and EHD2 del/+ adipocytes by staining with BODIPY (untreated:
522 n(del(+) = 74/3, n(del/del) = 60/3); differentiated: n(del/+) = 132/3, n(del/del) = 95/3). 3D reconstruction
523 of EHD2 del/del differentiated adipocyte (C). Green – LDs, blue – nucleus.
524 **D-E** Cultivated EHD2 cKO flox/wt or flox/flox adipocytes were transfected with Cre recombinase-EGFP to
525 induce EHD2 deletion and differentiated for 5 days, lipid droplets were stained with Nile Red for analyzing
526 (n(flox/wt) = 74/2, n(flox/flox) = 82/2).
527 **F-H** Fatty acid uptake assay in differentiated EHD2 del/+ and EHD2 del/del adipocytes. Dodecanoic acid-
528 BODIPY uptake was measured after 5, 10, 20, 30 or 60 min, and R1 population indicates positively stained
529 cells (illustrated in red in graph F). R2 populations (blue) correspond to higher BODIPY staining intensity
530 in cells and represent adipocytes with increased amount of dodecanoic acid taken up (shown in blue in
531 graphs F, H). Normalization of EHD2 del/del R2 population relative to EHD2 del/+ R2 (H, n(del/+) = 6/3
532 experiments, n(del/del) = 8/3 experiments). Example images of differentiated adipocytes treated with
533 dodecanoic acid for 60 min (G, scale bar 40 µm).
534 Column bar graphs illustrate mean +/- SE, t-test or Mann Withney U test were used to calculate
535 significance, * $P<0.05$; *** $P<0.0001$. See also Fig. S4 and S5.
536
537

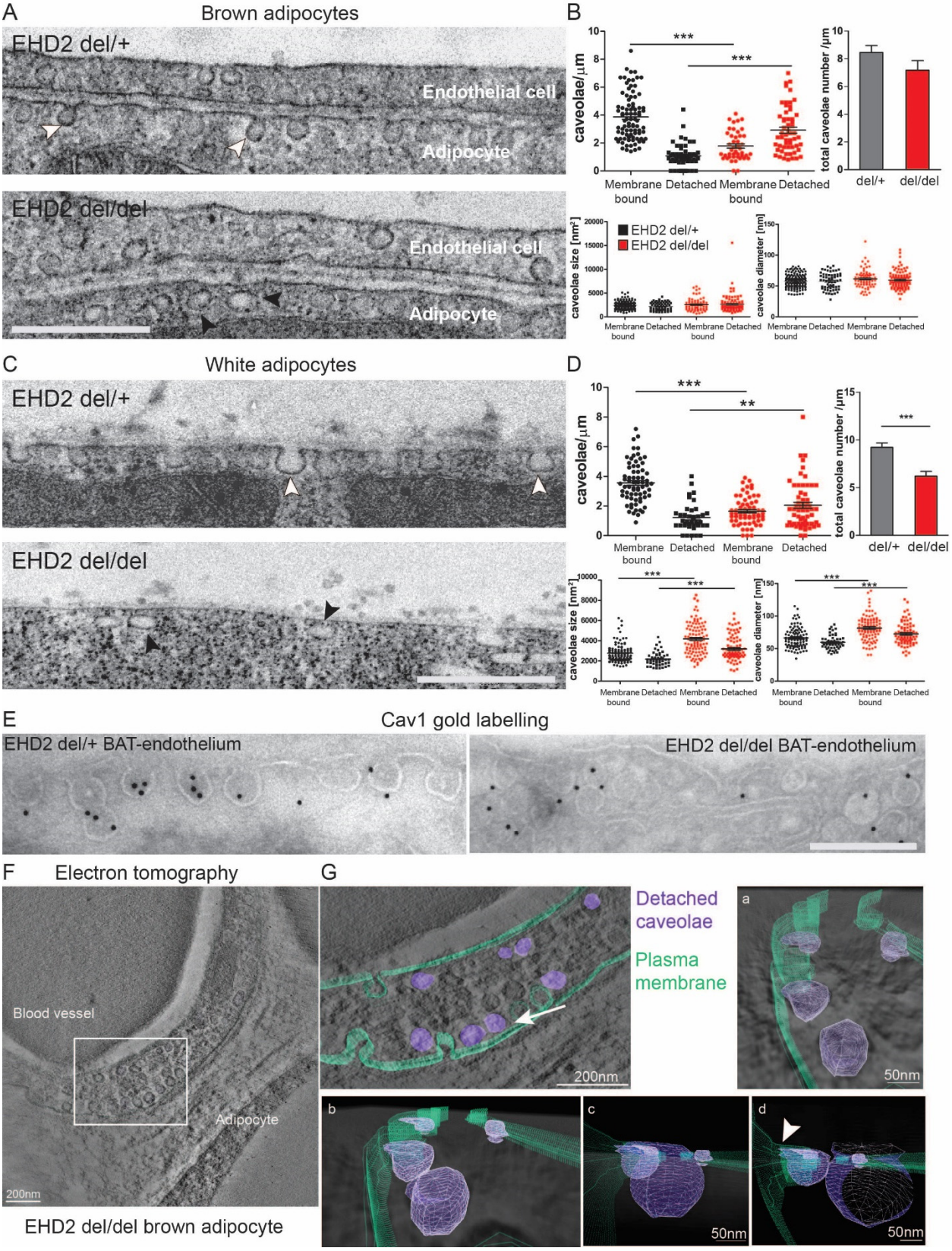

Fig. 3: Loss of EHD2 resulted in detached caveolae *in vivo*

540 **A-B** Representative EM images of BAT from EHD2 del/+ and del/del mice and systematic analysis (caveolae
541 number: n(del/+) = 140/3, n(del/del) = 100/3; caveolae size and diameter: n(del/+) = 201/3, n(del/del) =
542 171/3). Scale bar 500 nm.
543 **C-D** EM images of EHD2 del/+ and del/del WAT (caveolae number: n(del/+) = 108/3, n(del/del) = 124/3;
544 caveolae size and diameter: n(del/+) = 151/3, n(del/del) = 185/3). Scale bar 500 nm.
545 **E** Representative image for EM gold immunolabeling against Cav1. Control labeling did not reveal specific
546 staining. Scale bar 200 nm.
547 **F-G** Electron tomogram of a 150 nm EHD2 del/del BAT section (F). The 3D model contains the plasma
548 membrane (G, green) and the detached caveolae (violet). Detachment of caveolae was observed by
549 changing the viewing angle (white arrow indicates the direction). Closer inspection of cell membrane and
550 caveolae clearly showed displacement of caveolae from the membrane. The 3D model also revealed
551 attachment of caveolae to the membrane (arrow head).
552 Graphs illustrate each replicate with mean +/- SE, column bar graphs illustrate mean + SE t-test or Mann
553 Withney U test were used to calculate significance, ** P<0.001; *** P<0.0001. See also Movie S1
554

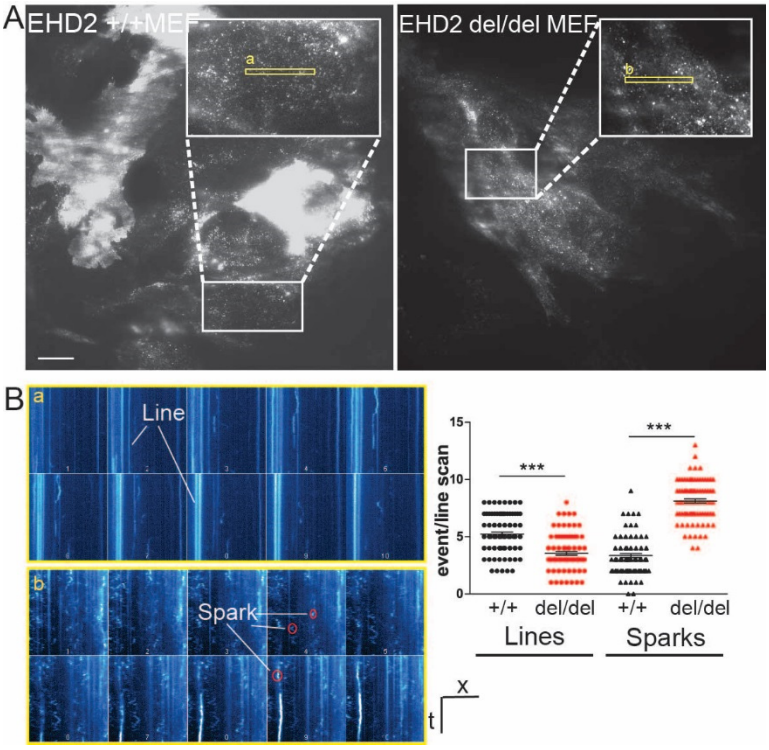

Fig. 4 Enhanced caveolar mobility in cells lacking EHD2

A-B TIRF live-imaging of EHD2 +/+ and del/del MEFs expressing pCav1-EGFP**.** Line scan analysis of the recorded Cav1 intensities revealed for fixed, non-moving caveolae lines and for fast moving caveolae single sparks (as illustrated in a and b, n(+/+) = 90/3; n(del/del) = 92/3; each replicate is represented with mean +/- SE), ***P<0.0001. See also Fig. S6 and Movie S2-4.

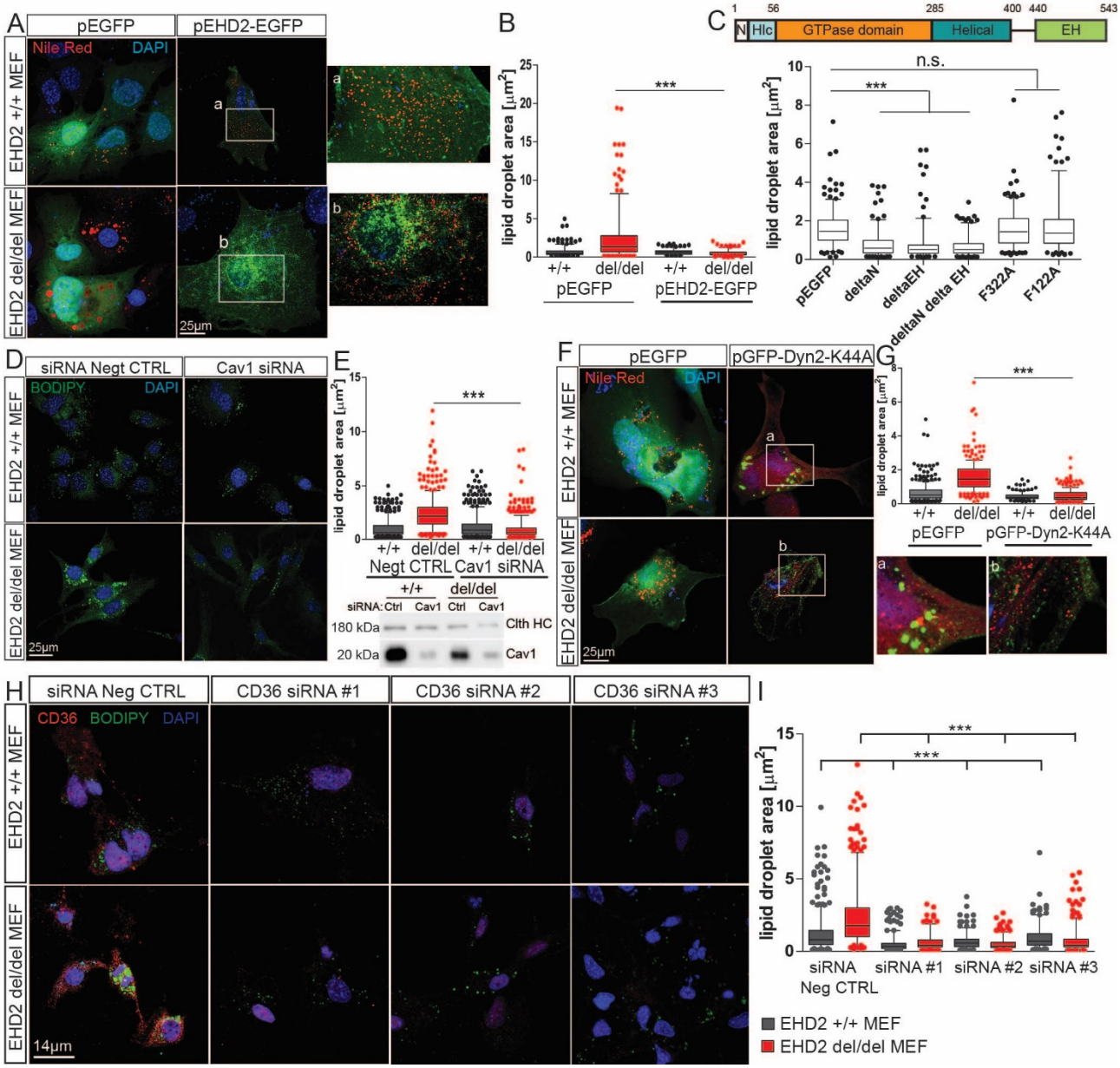

Fig. 5: EHD2-mediated fatty acid uptake depends on Cav1, Dyn2 and CD36

A-B EHD2 +/+ and del/del MEFs were transfected with either pEGFP or pEHD2-EGFP, incubated for 48 h and afterwards treated for 6 h with oleic acid and Nile Red staining was performed to determine LDs (pEGFP: n(+/+) = 309/3, n(del/del) = 310/3; pEHD2-EGFP: n(+/+) = 218/4, n(del/del) = 184/4).

C EHD2 constructs were transfected in EHD2 del/del MEFs and after 48h treated with oleic acid and Nile Red staining was performed to determine LDs (n(pEGFP) = 275/3; n(pEHD2-deltaN-EGFP) = 193/3; n(pEHD2-deltaEH-EGFP) = 197/3; n(pEHD2-deltaN-EH-EGFP) = 196/3; n(pEHD2-F322A-EGFP) = 204/3; n(pEHD2-F122A-EGFP) = 212/3).

D-E EHD2 del/del MEFs were treated with Cav1 siRNA and lipid droplets were stained with BODIPY (negative control: n(+/+) = 504/3, n(del/del) = 530/3; Cav1 siRNA: n(+/+) = 521/3, n(del/del) = 558/3); Clth HC - clathrin heavy chain.

573 **F-G** EHD2 +/+ and del/del MEFs were transfected with either pGFP-Dyn2-K44A, incubated for 18 h and
574 afterwards treated for 6 h with oleic acid and Nile Red staining was performed to determine LDs (pEGFP:
575 n(+/+) = 309/3, n(del/del) = 233/4; pGFP-Dyn2-K44A: n(+/+) = 136/3, n(del/del) = 237/4).
576 **H-I** LD size after CD36 siRNA knockdown in EHD2 +/+ and del/del MEFs (D, negative control: n(+/+) = 584/6,
577 n(del/del) = 475/6; CD36 siRNA#1: n(+/+) = 341/3, n(del/del) = 249/3; CD36 siRNA#2: n(+/+) = 412/3,
578 n(del/del) = 468/3; CD36 siRNA#3: n(+/+) = 251/3, n(del/del) = 368/3; graph illustrates each replicate with
579 mean +/- SE, 2-way ANOVA test were used to calculate significance between siRNA negative CTRL and
580 siRNA, t-test was used between +/+ and del/del data).
581 Box plots indicate mean +/- SE and single replicates of 5% of maximal and minimum values are illustrated,
582 t-test or Mann Withney U test were used to calculate significance, *** P<0.0001. See also Fig. S7.
583
584

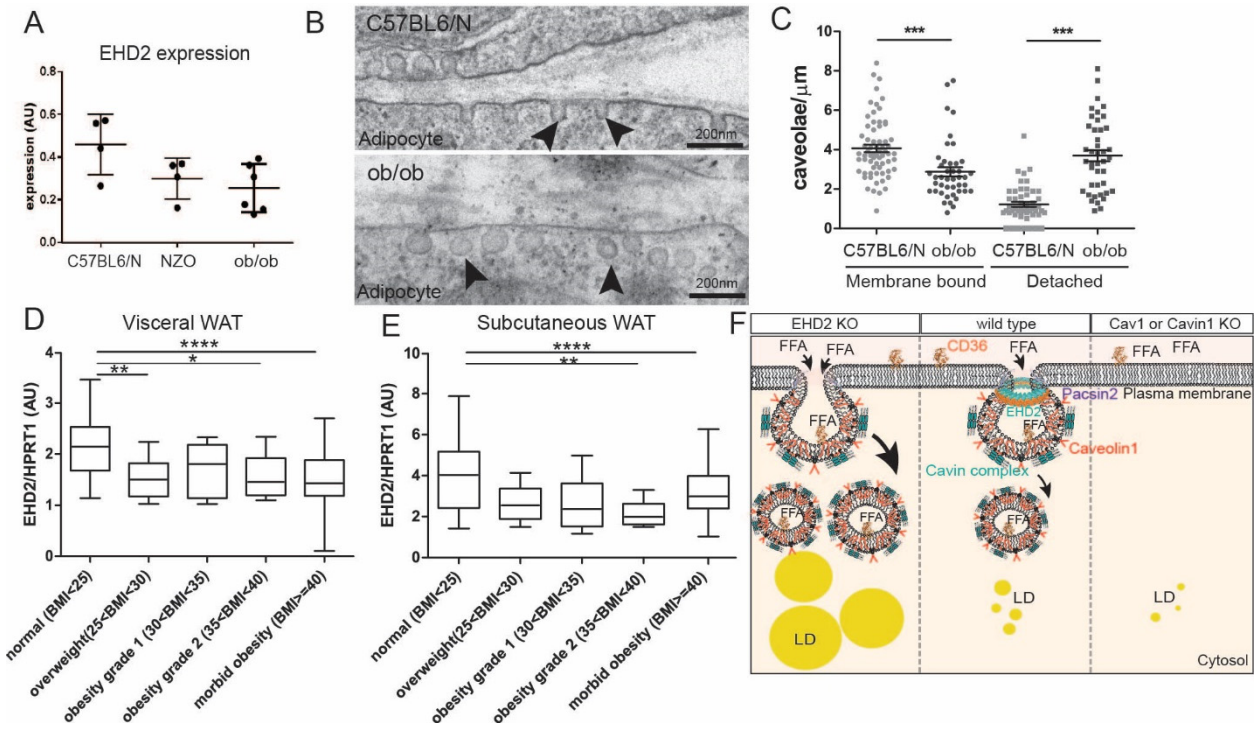

Fig. 6: Decreased EHD2 expression in diet induced obesity

A EHD2 expression level was analyzed in fat tissue of ob/ob or NZO mouse models compared to C57BL6/N mice (n = 5).

B-C Investigation of caveolae by EM imaging (n(ob/ob mice) = 85/2; n(C57BL6/N) = 117/2;).

D-E EHD2 expression in visceral (E) or subcutaneous WAT (F) in obese patients (n(normal) = 31; n(overweight) = 23; n(obesity grade 1) = 7; n(obesity grade 2) = 17; n(obesity grade 3) = 202).

F The model illustrates how fatty acid uptake is affected by caveolae function. In the absence of caveolae, lipid uptake is reduced resulting in smaller lipid droplets compared to normal conditions. In the absence of EHD2, lipid uptake is increased, suggesting a regulatory function of EHD2 in caveolae-dependent lipid uptake. FFA – Free fatty acid, LD – lipid droplet.

Box plots indicate median with whiskers from maximal to minimum value, or each replicate with mean +/- SE is represented, normal distributed groups were analyzed by t-test, not normal distributed values with Mann Withney U test, * P<0.05, *** P<0.0001.

601 **Supporting Information**

602 **Extended Material and Methods**

603 **Mouse embryonic fibroblast isolation and immortalization.** All animals were handled accordingly to
604 governmental animal welfare guidelines. MEFs were obtained from E14.5 EHD2 +/+ or del/del embryos.
605 Therefore female, pregnant EHD2 del/+ were sacrificed by cervical dislocation, the embryos were
606 dissected and removed from the yolk sac in sterile, cold PBS. For genotyping, a small piece of each mouse
607 embryo tail was harvested followed by complete dissection of the whole embryo. Afterwards, the embryo
608 pieces were treated with 0.25% trypsin/EDTA (Sigma) over night at 4 °C. After aspiration of the trypsin
609 solution, 10 ml culture medium (DMEM/10%FBS/5% penicillin/streptomycin) was added and tissue pieces
610 were break up by pipetting. The cell suspension was transferred in 75 cm^2 culture flask for cultivation at
611 37 °C and 5% CO_2. Immortalization of isolated primary MEFs was assured by frequently splitting. From
612 passage 15 an increased growth rate was observed suggesting immortalized MEFs. For all experiments
613 MEFs between passage 12 and 32 was used. For LD growth, MEFs were either treated with 10 µg/ml
614 insulin, 2.5 mM dexamethasone, 50 mM IBMX and 25 mM rosiglitazone (all obtained from Sigma) diluted
615 in culture medium (differentiation medium) or 0.016 M oleic acid and 10 µg/ml insulin diluted in DMEM.
616 **Primary adipocyte cell culture.** Male EHD2 del/+ and EHD2 del/del mice or EHD2 cKO flox/wt or flox/flox
617 were sacrificed by cervical dislocation and gonadal WAT was removed. Adipocytes and stromal vascular
618 fraction (SVF) were isolated after washing the tissue in sterile PBS and digestion by collagenase type II
619 (Sigma C6885). Mature adipocytes floating in the upper phase were transferred in a new flask and diluted
620 with culture medium (DMEM/10%FBS/5% penicillin/streptomycin), SVF was obtained after 5 min
621 centrifugation at 1,000 rpm. After complete tissue break up the adipocyte cell suspension was passed
622 through a 270 µm cell strainer and the cells were plated in 75 cm^2 culture flask at 37 °C and 5% CO_2
623 whereby pre-adipocytes adhere to the flask and mature adipocytes float in the medium. SVF suspension
624 was cleaned by passing through 70 µm cell strainer. The following day the culture medium was exchanged
625 to remove dead or non-adherent cells. After 5 days, both pre-adipocytes and SVF were split by 0.25%
626 trypsin/EDTA solution and merged for further cultivation. Differentiation to mature adipocytes was
627 induced by 10 µg/ml insulin, 2.5 mM dexamethasone, 50 mM IBMX and 25 mM rosiglitazone diluted in
628 culture medium. If not otherwise mentioned the primary pre-adipocytes were incubated for 5 days with
629 differentiation medium and medium was changed after 2 days. Delipidation of FBS was carried out as
630 described by (1). EHD2 cKO adipocytes were transfected with Cre recombinase-EGFP by using adeno-

631 associated virus particles 8 (AAV8) produced from pAAV.CMV.HI.eGFP-Cre.WPRE.SV40 (addgene,
632 #105545). The adipocyte cell culture was transfected and differentiated for 5 days.
633 **Oil Red O staining.** LDs in tissue sections or cultivated adipocytes and MEFs were stained with Oil Red O
634 (Sigma #O0625) as published by (2). Briefly, freshly dissected liver of muscle pieces were frozen in liquid
635 nitrogen, embedded in TissueTek and 10 µm cryostat sections (Leica) were prepared. After fixation with
636 4% para-formaldehyde (PFA, Merck) freshly prepared Oil Red O staining solution was applied for 10 min.
637 The sections were washed with PBS and embedded in ImmoMount (Invitrogen). Cultivated cells were
638 fixed, treated with 60% isopropanol (Merck) for 2 min and then incubated with Oil Red O staining solution
639 for 5 min. After washing with water until complete removal of Oil Red O the stained cells or sections were
640 analyzed by Zeiss Axiovert microscope (20x Zeiss objective). Staining intensity was measured with ImageJ.
641 **Histology.** EHD2 del/+ and EHD2 del/del mice were anesthetized with 2% ketamine/10%rompun, perfused
642 first by 30 ml PBS and next by 50 ml 4% PFA and tissues were dissected. After 24 h of fixation in 4% PFA,
643 tissues were dehydrated in 3 steps (each 24h) from 70-100% EtOH and afterwards incubated in xylol
644 (Merck) for 48 h. Next, the tissues were embedding in liquid paraffin at ca. 65°C and cooled down on ice.
645 4 µm paraffin sections were obtained, de-paraffinized and hydrated and Masson Trichrome staining (Kit,
646 Sigma) was applied. Briefly, sections were stained with Bouin solution for 15 min at 60°C, followed by
647 Haematoxylin Gill No. 2 staining for 5 min and incubation in Biebrich-Scarlet-Acid Fuchsin for 5 min. Next,
648 the tissue sections were treated with Phosphotungstic/Phosphomolybdic Acid Solution and Aniline Blue
649 solution both for 5 min, and acetic acid treatment (1%) for 2 min. After extensive washing the sections
650 were dehydrated, incubated in xylol and embedded with Roti Histo Kit (Carl Roth). Images were obtained
651 at Zeiss Axiovert100 microscope.
652 **Immunohistostaining of cryostat sections.** Perfused and fixated EHD2 del/+ and EHD2 del/del mice (as
653 described before) were dissected and the investigated tissue pieces were further fixed for 1-4 h in 4% PFA,
654 transferred to 15% sucrose (in PBS, Merck) for 4 h and finally incubated overnight in 30% sucrose. After
655 embedding in TissueTek, the tissue is frozen at -80 °C. 5-15 µm sections were obtained in a cryostat at -
656 20 - -30 °C and stored at -20 °C. For immunostainings, the cryostat sections were incubated with blocking
657 buffer (1% donkey serum/1% TritonX100/PBS) for 1 h at room temperature, and treated overnight at 4°C
658 with the first antibody diluted in blocking buffer. After washing with PBS/1%Tween, the secondary
659 antibody was applied for 2 h at room temperature. After completion of the staining, the sections were
660 washed carefully and embedded in ImmoMount. The stained sections were analyzed with Zeiss LSM700
661 microscope provided with Zeiss objectives 5, 10, 20, 40 and 63x. The obtained images were further
662 investigated by ZEN software and ImageJ/Fij.

663 **Transfection and siRNA knockdown.** Cultivated MEFs were transfected with the following plasmids
664 pEHD2-EGFP, pEHD2-deltaN-EGFP, pEHD2-deltaEH-EGFP, pEHD2-deltaN-EH-EGFP, pEHD2-F322A-EGFP,
665 pEHD2-F122A-EGFP, pCav1-EGFP (provided from R.L.), pGFP-Dyn2-K44A (provided from M.L., addgene
666 #22301) or pEGFP by lipofectamine 3000 (Invitrogen) accordingly to the manufacture's protocol.
667 Transfected cells were incubated for 48 h and afterwards the treated cells were analyzed by confocal
668 microscopy or TIRF. siRNA knockdown of CD36 or Cav1 was performed in freshly split MEFs by
669 electroporation with the GenePulser XCell (Biorad). Briefly, MEFs were split as described before and the
670 obtained cell pellet was resuspended in OptiMEM (Gibco). After cell counting, the MEF cell suspension
671 was diluted to $1.5x10^6$ cells/ml and 300 µl were transferred into electroporation cuvettes (2 mm, Biorad).
672 CD36 or Cav1 stealth siRNA and siRNA negative control (medium GC content, CD36 siRNA#1
673 GGAAUUUGUCCUAUUGGCCAAGCUA, CD36 siRNA#2 CCAAGUCUUCUAUGUUCCAAACAAG; CD36 siRNA#3
674 CCAAUAACUGUACAUCUUAUGGUGC) was added to a final concentration of 200 nM. After carful mixing,
675 the cuvettes were placed into the electroporation device and the pulse (160 µOHM, 500 µF, ∞ resistance)
676 was applied. The electroporated cells were cultivated in DMEM/10%FBS for 48 h before the experiments
677 were started. Successful siRNA knockdown was monitored by CD36 antibody staining.
678 **TIRF live imaging of caveolae movement.** MEFs transfected with pCav1-EGFP were incubated for 48 h on
679 fibronectin coated cover slips (25 mm diameter). Samples were mounted in Attofluor Cell Chamber
680 (Thermo) in a physiological buffer (130 mM NaCl, 4 mM KCl, 1.25 mM NaH_2PO_4-H_2O, 25 mM $NaHCO_3$, 10
681 mM glucose, 2 mM $CaCl_2$, 1 mM $MgCl_2$, pH 7.3, 305-315 mOsm/kg).
682 TIRF imaging was performed on an inverted Microscope (Nikon Eclipse Ti) equipped with a 488 laser
683 (Toptica), an dicroic mirror (AHF, zt405/488/561/640 rpc), a 60x TIRF objective (Nikon, Apo TIRF NA 1.49),
684 an appropriate emission filter (AHF, 400-410/488/561/631-640) and a sCMOS camera (mNeo, Andor). All
685 components were operated by open-source ImageJ-based micromanager software. All experiments were
686 performed at 37 °C. To investigate the movement of single caveolae transfected cells were selected in
687 which regions of individual Cav1 spots were observed (ROIs illustrated in Fig. 4A, enhanced images).
688 Recordings were obtained with the following imaging settings: image size 1776x1760 pixel, 1x1 binning,
689 500 frames, 200 ms exposure time/frame. For data analysis only the first 150 frames were investigated.
690 After cropping to the specific ROI, kymograph analysis of several positions within the ROIs were carried
691 out using the Reslice function of ImageJ/Fij. Carefully investigation of the kymographs revealed a single,
692 straight line for fixed, not moving caveolae and sparks or short lines for fast moving caveolae.
693 **Transmission Electron microscopy (TEM).** Mice were fixed by perfusion with 4% (w/v) formaldehyde in
694 0.1 M phosphate buffer and tissues were dissected to 1-2 mm^3 cubes. For morphological analysis, tissue

695 blocs were postfixed in phosphate buffered 2.5% (v/v) glutaraldehyde. Samples were treated with 1%
696 (v/v) osmium tetroxide, dehydrated in a graded series of ethanol and embedded in the PolyBed® 812 resin
697 (Polysciences Europe GmbH). Ultrathin sections (60-80 nm) were cut (Leica microsystems) and stained
698 with uranyl acetate and lead citrate before image acquisition. For immuno-labeling, samples were fixed
699 by perfusion as described above, but postfixed in phosphate buffered 4% (w/v) formaldehyde with 0.5%
700 (v/v) glutaraldehyde for 1 hour. Samples were further processed as described in Slot and Geuze (Nature
701 protocols, 2007). Briefly, samples were infiltrated with 2.3 M sucrose, frozen in liquid nitrogen and
702 sectioned at cryo temperatures. Sections were blocked and washed in PBS supplemented with 1% BSA
703 and 0.1% glycine. Labeling was performed with an anti-caveolin-1 antibody 1:500 (abcam #2910) and 12
704 nm colloidal gold (Dianova). Sections were contrasted with 3% tungstosilicic acid hydrate (w/v) in 2.8%
705 polyvinyl alcohol (w/v) (3). Samples were examined at 80 kV with a Zeiss EM 910 electron microscope
706 (Zeiss). Acquisition was done with a Quemesa CDD camera and the iTEM software (Emsis GmbH).
707 ***In situ* hybridization.** Digoxigenin-labeled riboprobes were generated using a DIG-RNA labeling kit
708 (Roche). In situ hybridizations were performed on 14 µm cryosections prepared from E18.5 wt embryos
709 as previously described (4). To generate an Ehd2 specific in situ probe, a 400 bp fragment was amplified
710 from wildtype cDNA using PCR and primer listed below. The PCR product was cloned into pGEM-Teasy
711 (Promega). T7 and sp6 polymerases were used to generate Ehd2-sense and antisense probes,
712 respectively. EDH2_ISH_FWD: 5'-CAGGTCCTGGAGAGCATCAGC-3'**;** EDH2_ISH_REV: 5'-
713 GAGGTCCTGTTCCTCCAGCTCG-3'
714 **Western Blot.** EHD2 protein level in different tissues was examined by Western Blot. Therefore EHD2 +/+,
715 EHD2 del/+ and EHD2 del/del mice were sacrificed by cervical dislocation and organs were dissected and
716 snap frozen in liquid nitrogen. After homogenization of the tissue in 1x RIPA buffer (Abcam) with a glass
717 homogenizer, the tissue lysate was incubated for 1 h on ice followed by 15 min centrifugation at 15,000
718 rpm. Supernatant was transferred in a fresh tube and protein concentration was measured by NanoDrop.
719 At least 10 µg protein/lane was applied to 4-12% SDS-PAGE NuPage (Invitrogen) and SDS-PAGE was
720 performed accordingly to the manufacture's protocol. Afterwards, proteins were blotted on nitrocellulose
721 membrane (Amersham) at 80 V for 1 h, followed by blocking of the membranes with 5% milk powder (in
722 TBST, 150 mM NaCl, 20 mM Tris-HCl, pH 7.5, 0.1% Tween20) for 2 h at room temperature. To detect EHD2
723 protein level rabbit-anti-EHD2 (1:2,000) was applied over night at 4 °C. After washing with TBST the
724 secondary antibody goat-anti-rabbit-HRP was added to the membrane for 2 h at room temperature.
725 Detection of EHD2 bands results from ECL detection solution and intensities were obtained by ChemiDoc
726 XRS (Biorad).

727 **Antibodies.** Anti-EHD2-Rb (self-made), anti-Cav1-Mouse (BD Biosciences #610407), anti-Rabbit IgG HRP
728 (dianova), anti-Mouse IgG HRP (dianova), anti-Perilipin1-Rb (Cell signaling #9349), anti-CD36-Rb (Novus
729 Bio #NB400-144 and abcam #ab133625), anti-Cavin1-Rb (Abcam, #ab48824), anti-Rb-Cy3 (dianova), anti-
730 mouse IgG-Alexa488 (ThermoScientific #R37114), DAPI (Sigma D9542)
731 **Blood plasma analysis.** To measure distinct blood plasma parameter related to metabolic changes like
732 adiponectin, insulin or free fatty acids blood was taken from EHD2 del/+ and EHD2 del/del mice
733 immediately after cervical dislocation. All blood samples were taken at 10.00 am. Briefly, mice were
734 opened and the thorax was partly removed to get access to the left heart ventricle, a cannula was inserted
735 and blood samples were taken. After short centrifugation at high speed, the plasma fraction was
736 transferred to a fresh tube and snap frozen in liquid nitrogen. The following assays were used to measure
737 the described blood plasma markers: Plasma insulin levels were measured by Mouse Ultrasensitive Insulin
738 ELISA (80-INSMSU-E10, Alpco). Plasma adiponectin and leptin levels were measured by Mouse
739 Adiponectin/Acrp30 (DY1119) and Mouse/Rat Leptin (MOB00) ELISA kits (R&D Systems). Plasma lipids
740 were quantified with commercially available kits: cholesterol (Cholesterol liquicolour colorimetric assay,
741 Human, Wiesbaden, Germany), triglycerides/glycerol (Triglyceride/Glycerol Calorimetric Assay, Sigma)
742 and non-esterified fatty acids (Wako Chemicals). All measurements were done according to
743 manufacturers' recommendations.
744 **Fatty acid uptake assay.** EHD2 del/+ and EHD2 del/del pre-adipocytes were seeded in 6-well plates
745 (100.000 cells/well) and differentiated in mature adipocytes as described above. The fatty acid uptake
746 assay was performed as described elsewhere (5). Briefly, after 5 days of differentiation, adipocytes were
747 starved for 1 h with serum-free DMEM. Next, 2 µM dodecanoic acid (FA12) labelled with BODIPY
748 (Molecular probes #D3822) diluted in serum-free DMEM + 10 µg/ml insulin was added to the adipocytes
749 and incubated for 5, 10, 20, 30 and 60 min at 37 °C. After washing twice with ice-cold PBS, 150 µl 0.25%
750 trypsin/EDTA/PBS was applied to detach the cells. The adipocytes were treated with 500 µl ice-cold FACS
751 buffer (HBSS/10%FBS/10 mM EDTA) and the cell solution was transferred to FACS tubes. Shortly before
752 measurement, 1 µl/ml propidium iodide was added. FACS experiments were performed at LSR Fortessa
753 5Laser with the following parameters: FSH: A, H, W, Voltage 255; SSC: A, H, W, Voltage 203; A488: A,
754 Voltage 198; PE: A, Voltage 341. For each FACS sample 30.000 cells were investigated. As negative control
755 unstained EHD2 del/+ and EHD2 del/del adipocytes were examined at first and the obtained BODIPY
756 intensity values were used as a reference for unstained cells. To exclude adipocytes which did not show
757 any positive fatty acid uptake, all unstained cells were removed resulting in an only positive stained
758 population (R1, illustrated in red in Fig. 2F). Within this R1 population adipocytes with strongly increased

759 BODIPY intensity values were gated to population R2 (blue, Fig. 2F). Detailed analysis/gating and statistics
760 was done by using FlyingSoftware2.5.1 (Perttu Terho, Cell Imaging Core, Turku Center for Biotechnology).
761 For each experiment 15.000 cells were analyzed and gated to the unstained, R1 or R2 population. Next,
762 the percentage of the cells gated to the populations were calculated for every time point and illustrated
763 in the bar graph (Fig. S4C). R2 population was investigated in more detail by normalization to the R2 cell
764 number of EHD2 del/+ adipocytes (Fig. 2H).
765 **Glucose uptake assay.** Glucose uptake of EHD2 del/+ and EHD2 del/del adipocytes was measured as
766 described by BioVison (2-NBDG Glucose uptake assay). Briefly, adipocytes were treated as described for
767 fatty acid uptake assay. However, after starvation 200 µM 2-NBDG (2-deoxy-2-[(7-nitro-2,1,3-
768 benzoxadiazol-4-yl) amino]-D-glucose, molecular probes #N13195) diluted in serum-free DMEM + 10
769 µg/ml insulin was applied to the cells followed by incubation times from 5-60 min. Staining analysis was
770 done as mentioned for fatty acid uptake with the same FACS parameters and gating procedure whereby
771 only one positive stained cell population was examined (R1, illustrated in Fig. S4E).
772 **Gene expression analysis.** EHD2 del/+ and EHD2 del/del adipocytes were differentiated for 5 days,
773 washed twice with ice-cold PBS and RNA was isolated accordingly to the Qiagen protocol (RNeasy Mini
774 Kit, Qiagen). SuperscriptIII First Strand Synthesis Kit (Invitrogen #18080051) was used to obtain
775 corresponding cDNA, which then was used for real-time PCR. Gene expression levels were analyzed by
776 GoTaq q-PCR (Promega, #A6001) Master Mix in Fast real time PCR cycler (Applied Biosystems) accordingly
777 to instructor's protocol. To measure the relative fold change of genes in EHD2 del/del adipocytes
778 compared to EHD2 del/+, the comparative real-time PCR method was applied whereby actin was used as
779 reference gene.
780 Total mRNA from murine gonadal adipose tissue (gWAT) was extracted with RNeasy Mini Kit (QIAGEN
781 GmbH, Hilden) according to manufacturer's instructions. RNA was transcribed using the Moloney Murine
782 Leukemia Virus Reverse Transcriptase (M-MLV RT, Promega) according to manufacturer's
783 recommendations. Expression of mRNA was determined by quantitative real-time PCR on LightCycler 480
784 II/384 (Roche, Rotkreuz, Switzerland) using GoTaq Probe qPCR Master Mix (Promega, Madison, USA)
785 applying TaqMan Gene Expression Assays. Target gene expression of was normalized to the mean
786 expression of *Eef2*, *Ppia* and *Actb* in murine samples.

Gene	**Description**	**TaqMan Assay**
EHD2	EH-domain containing 2	Hs.PT.58.4969281
Ehd2	EH-domain containing 2	Self-designed
Actb	Actin, beta	Self-designed

Eef2	Eukaryotic translation elongation factor 2	Self-designed
Ppia	Peptidylprolyl isomerase A	Mm.PT.39a.2.gs

787 ***Actb*** Left primer: TACGACCAGAGGCATACAG, Right primer: GCCAACCGTGAAAAGATGAC, Probe:
788 TTGAGACCTTCAACACCCCAGCCA, ***Eef2*** **(Integrated DNA Technologies)** Left primer:
789 CACAATCAAATCCACCGCCA**,** Right primer: TGAGGTTGATGAGGAAGCCC**,** Probe:
790 TAAGCAGAGCAAGGATGGCT**,** ***Ehd2*** **(UPL, Roche)** Left primer: CAGCTGGAGCACCACATCT**,** Right primer:
791 TCATGTGCCATCAACAGCTC**,** UPL probe: #80

792 **Lipid composition.** The measurement of lipid amount and its composition in tissue samples or cells were
793 performed by Lipotype GmbH (Dresden, Germany). For this, tissue samples were homogenized
794 accordingly to the supplied Lipotype protocol and diluted samples (1 mg/ml) were frozen and analyzed by
795 Lipotype. MEF were split and the cell pellet was diluted in cold PBS to a final cell number of 30,000 cells/ml.
796 **Statistical analysis.** At first, a normality distribution test (Kolmogorov-Smirnov test) was carried out for all
797 experimental values. If the data was normally distributed, Student t-Test (two-tailed P-value) was applied,
798 otherwise Mann-Withney-Rank-Sum (two-tailed P-value) test was used to calculate the significant
799 difference between two groups. Two-way-Anova tests were used to investigate LD size after CD36 siRNA
800 knockdown, whereby for EHD2 wt and KO MEFs each CD36 siRNA#1-3 treated cells were compared to
801 nonsense siRNA (negative control, Fig. 5I). Box plots, if not otherwise indicated in the figure legends,
802 always represents median with whiskers from minimum to maximum, column bar graphs and line graphs
803 represent mean with mean standard error of the mean (SE). Statistical calculations were carried out by
804 using Prism (GraphPad software). Distribution of LD sizes represented in histograms were also obtained
805 by using Prism. For all experiments including the examination of mice or mouse tissue or human samples,
806 n represents the number of mice/patients which were used (Fig. 1, 3, 6, S1-5) and all analyzed
807 cryo/paraffin sections or caveolae are also indicated (e.g.: n = 80 caveolae/3 mice). In cell culture
808 experiments (Fig. 2, 4, 5, S4-7), n represents the number of investigated events (e.g.: lipid droplet area)
809 and the number of independently performed experiments (e.g.: n = 80 lipid droplets/3 independent
810 experiments). The following P-values were used to indicate significant difference between two groups: *
811 P<0.05; ** P<0.001; *** P<0.0001.
812

813 ## Supplemental Material

814 **Movie S1: Electron tomography of EHD2 del/del BAT (related to Fig. 3)**

815 Caveolae in a 150 nm EHD2 del/del BAT section were investigated by electron tomography. The movie
816 includes all images obtained during the tilting from -60° to 60° (image acquisition every 2°). Both, detached
817 and plasma membrane bound caveolae can be observed. For better handling during the segmentation
818 and reconstruction in IMOD, the tomogram was reflected horizontal.

819 **Movie S2-3: TIRF live imaging of caveolae in EHD2 +/+ and del/del MEFs (related to Fig. 4)**

820 EHD2 +/+ and del/del MEFs were transfected with pCav1-EGFP to detect single caveolae and afterwards
821 TIRF live imaging was performed. Movie S2 illustrates an example EHD2 +/+ MEF, and Movie S3 shows an
822 EHD2 del/del MEF. Notably, Cav1 spots in MEFs lacking EHD2 showed increased caveolar dynamics.

823 **Movie S4: TIRF live imaging of caveolae in EHD2 del/del MEFs transfected with pEHD2-EGFP (related to**
824 **Fig. 4)**

825 EHD2 del/del MEFs were co-transfected with pCav1-EGFP and pEHD2-EGFP and caveolae movement was
826 observed by TIRF live imaging. Re-expression of EHD2 in EHD2 del/del MEFs strongly reduced the
827 dynamics of caveolae.

828

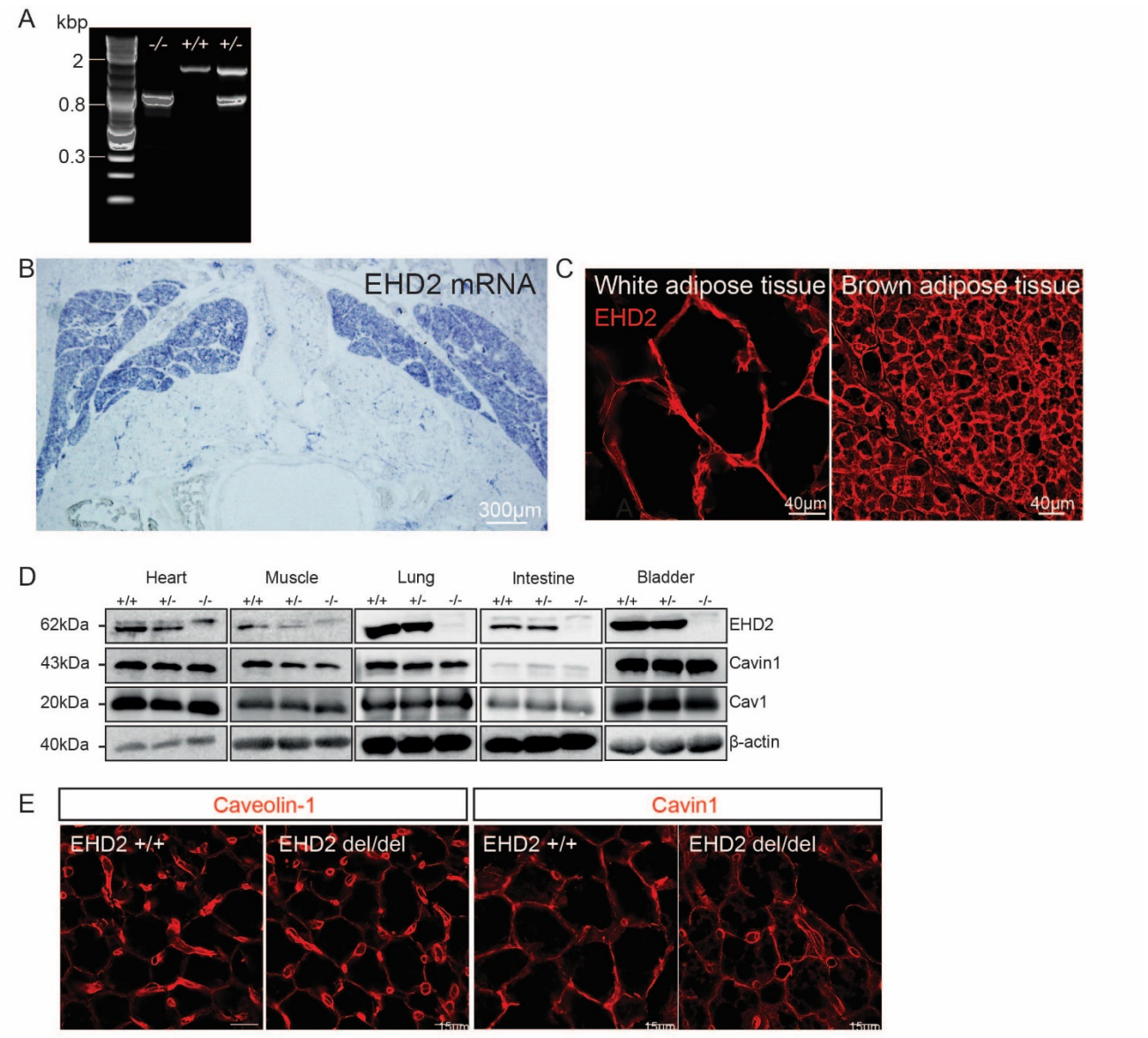

Fig. S1: EHD2, Cav1 and Cavin1 expression in BAT (related to Fig. 1)

A Genotyping of EHD2 delta E3 offspring (wildtype – band size 1,700 bp; EHD2 KO – band size 830 bp).
B *In situ* hybridization against EHD2 mRNA of BAT in an E18 C57BL6/N embryo.

C Cryostat section of adult C57BL6/N white adipose or brown adipose tissue stained against EHD2.
D Western Blot analysis of different tissues from EHD2+/+, +/- and -/- mice showing EHD2, Cav1 and Cavin1 protein level.

E Cavin1 and Cav1 protein level in BAT cryostat sections from EHD2 wt and del/del mice.

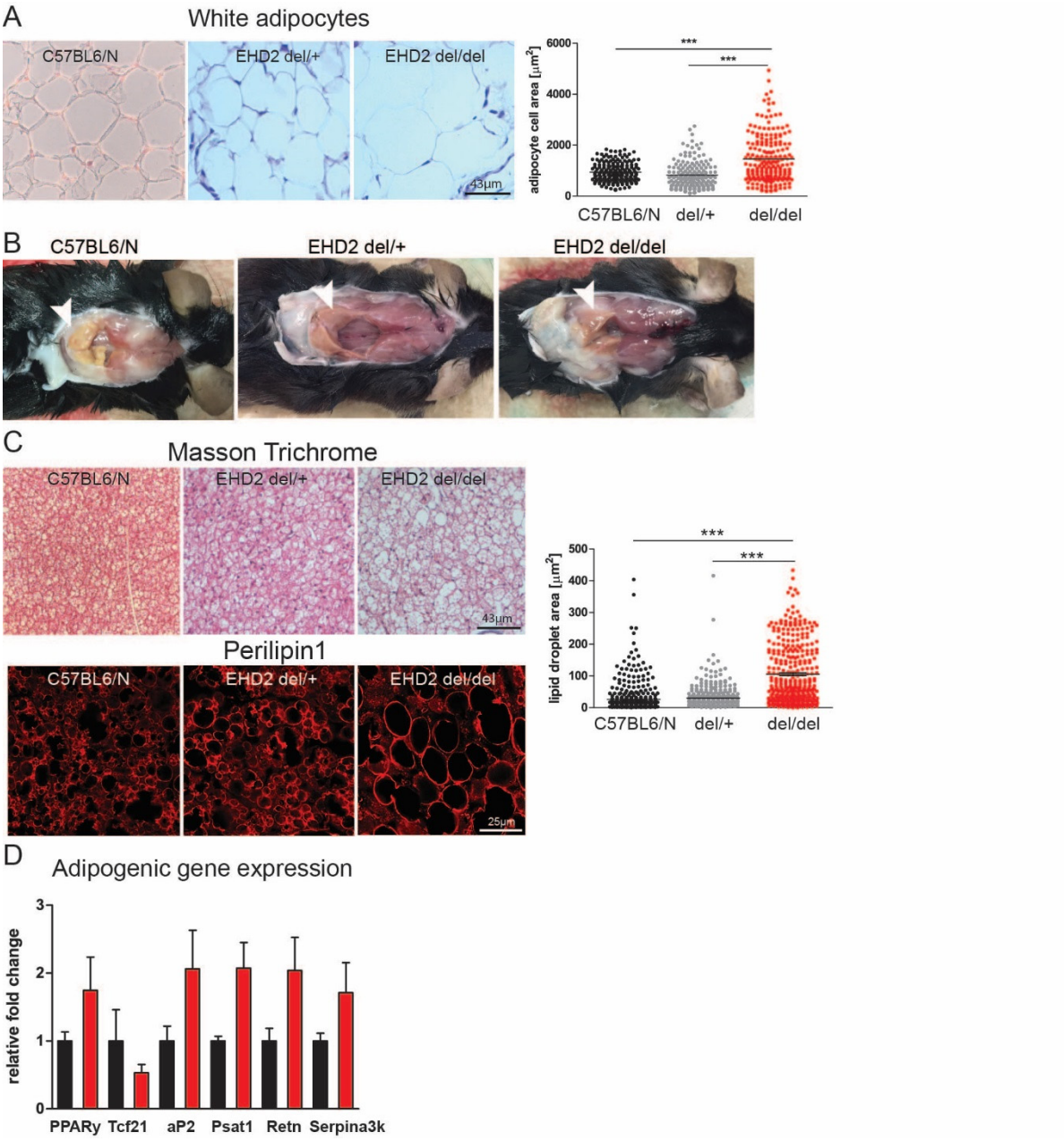

Fig. S2: C57BL6/N and EHD2 del/+ mice did not reveal any differences in lipid accumulation (related to Fig. 1)

A WAT paraffin sections from C57BL6/N mice stained with Masson Trichrome and analyzed by adipocyte cell size (n(C57BL6/N) = 186/3; n(EHD2 del/+ = 172/3; n(EHD2 del/del) = 199/3).

B BAT examples of C57BL6/N, EHD2 del/+ and del/del mice.

C BAT paraffin and cryostat sections stained against Perilipin1 obtained from C57BL6/N mice (lipid droplet size was measured by Perilipin1 staining, n(C57BL6/N) = 461/3; n(EHD2 del/+ = 398/3; n(EHD2 del/del) = 352/3).

D Adipogenic gene expression analysis of WAT from EHD2 del/+ and EHD2 del/del mice (n = 8).

Graphs illustrate each replicate with mean +/- SE, column bar graphs show mean + SE, normal distributed groups were analyzed by t-test, not normally distributed values with Mann Withney U test, * $P<0.05$, *** $P<0.0001$.

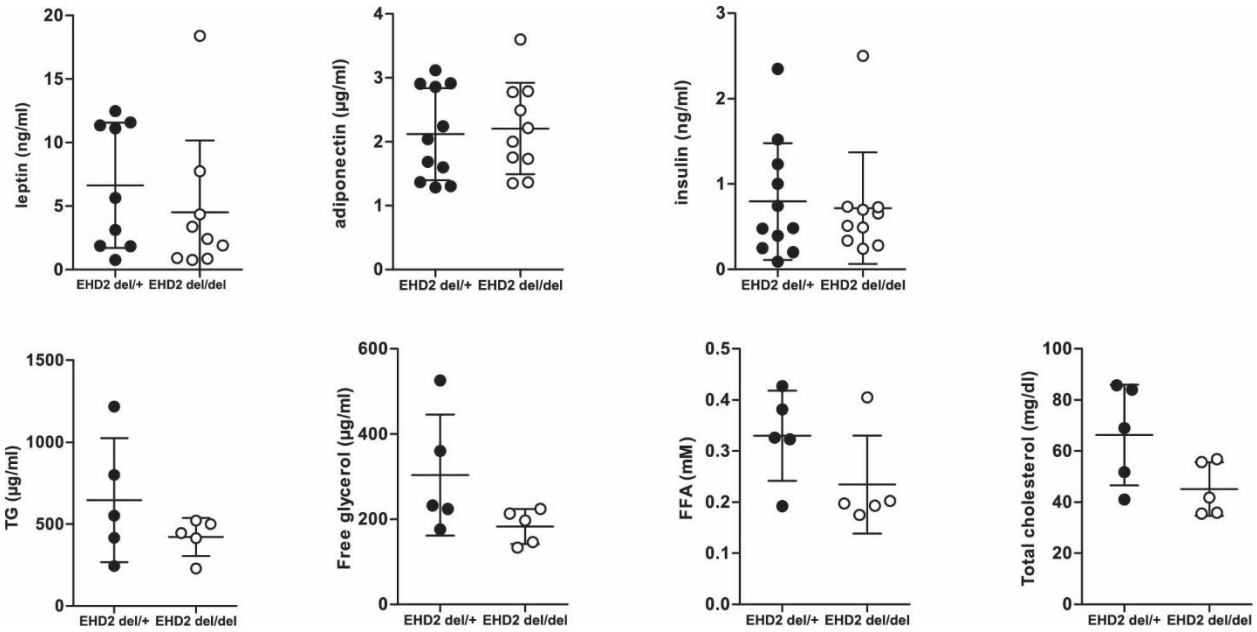

Fig. S3: Blood plasma analysis of EHD2 del/+ and EHD2 del/del mice did not reveal any significant differences (related to Fig. 1)

Blood samples obtained from EHD2 del/+ and del/del mice (n(EHD2 del/+) = 10 or 5; n(EHD2 del/del) = 10 or 5; graph illustrates each replicate with mean +/- SE). FFA – free fatty acid, TG – triglycerol.

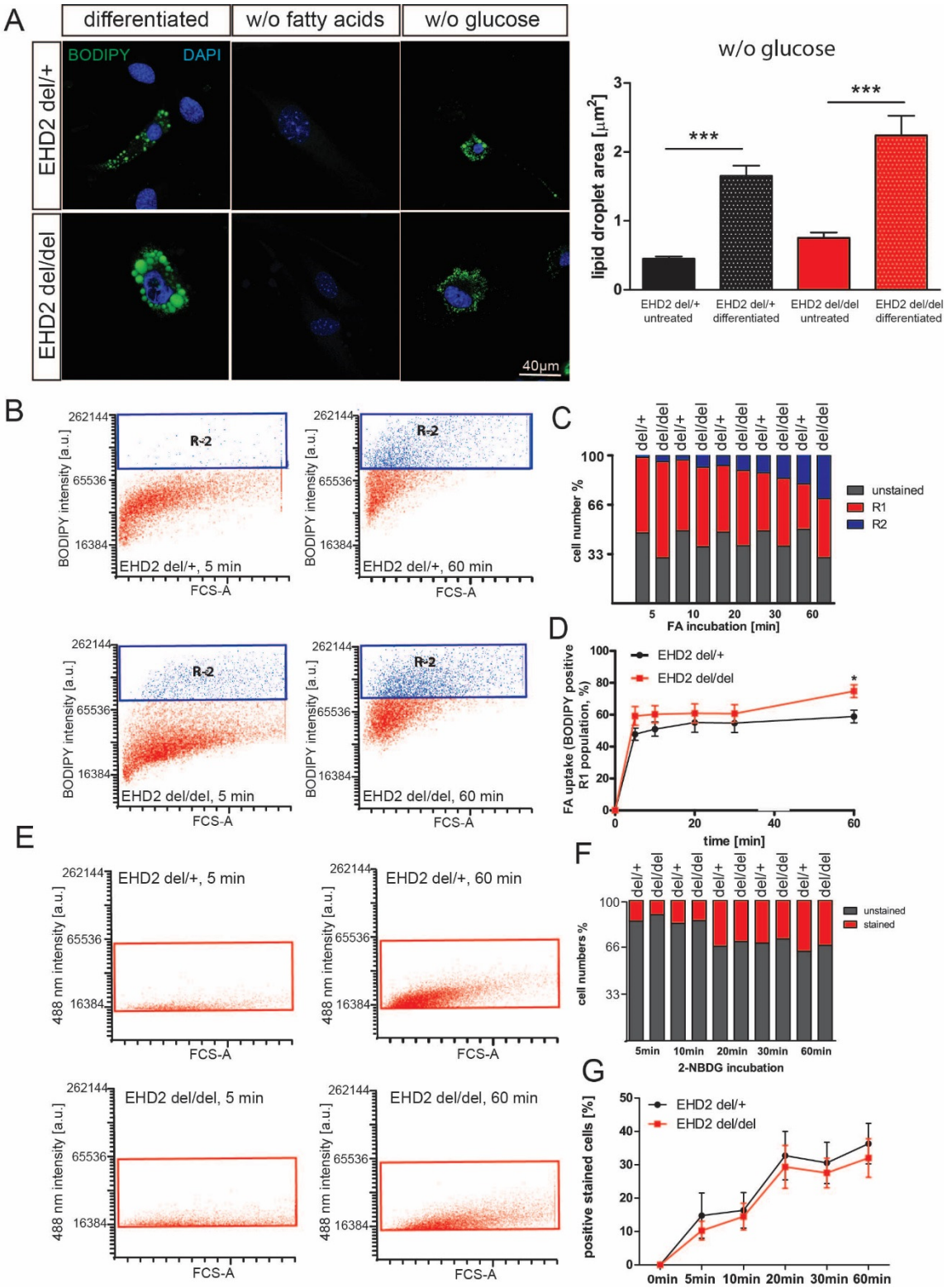

858

859 **Fig. S4: Cellular investigation of EHD2 del/del adipocytes (related to Fig. 2)**

860

861

862 **Fig. S4: Cellular investigation of EHD2 del/del adipocytes (related to Fig. 2)**

863 **A** Pre-adipocytes were treated with either differentiation medium containing delipidated FBS or without
864 glucose and BODIPY staining illustrating LDs.
865 **B-D** Fatty acid uptake assay in differentiated EHD2 del/+ and EHD2 del/del adipocytes. Dodecanoic acid-
866 BODIPY uptake was measured after 5, 10, 20, 30 or 60 min, and R1 population indicates positively stained
867 cells (illustrated in red in graphs B, C). R2 populations (blue) correspond to higher BODIPY staining
868 intensity in cells and represent adipocytes with increased amount of dodecanoic acid taken up (shown in
869 blue in graphs B, C). Overview of fatty acid uptake (percent cell numbers (B), and time scale (D); B-D,
870 n(del/+) = 6/3 experiments, n(del/del) = 8/3 experiments).
871 **E-G** Following 5 days of differentiation, glucose uptake in cultured adipocytes was measured after 5-60
872 min (C, n = 6).

873 Line graphs show mean +/- SE, column bar graphs show mean + SE , t-test or Mann Withney U test was
874 used to calculate significance, ** P<0.001, *** P<0.0001.

875

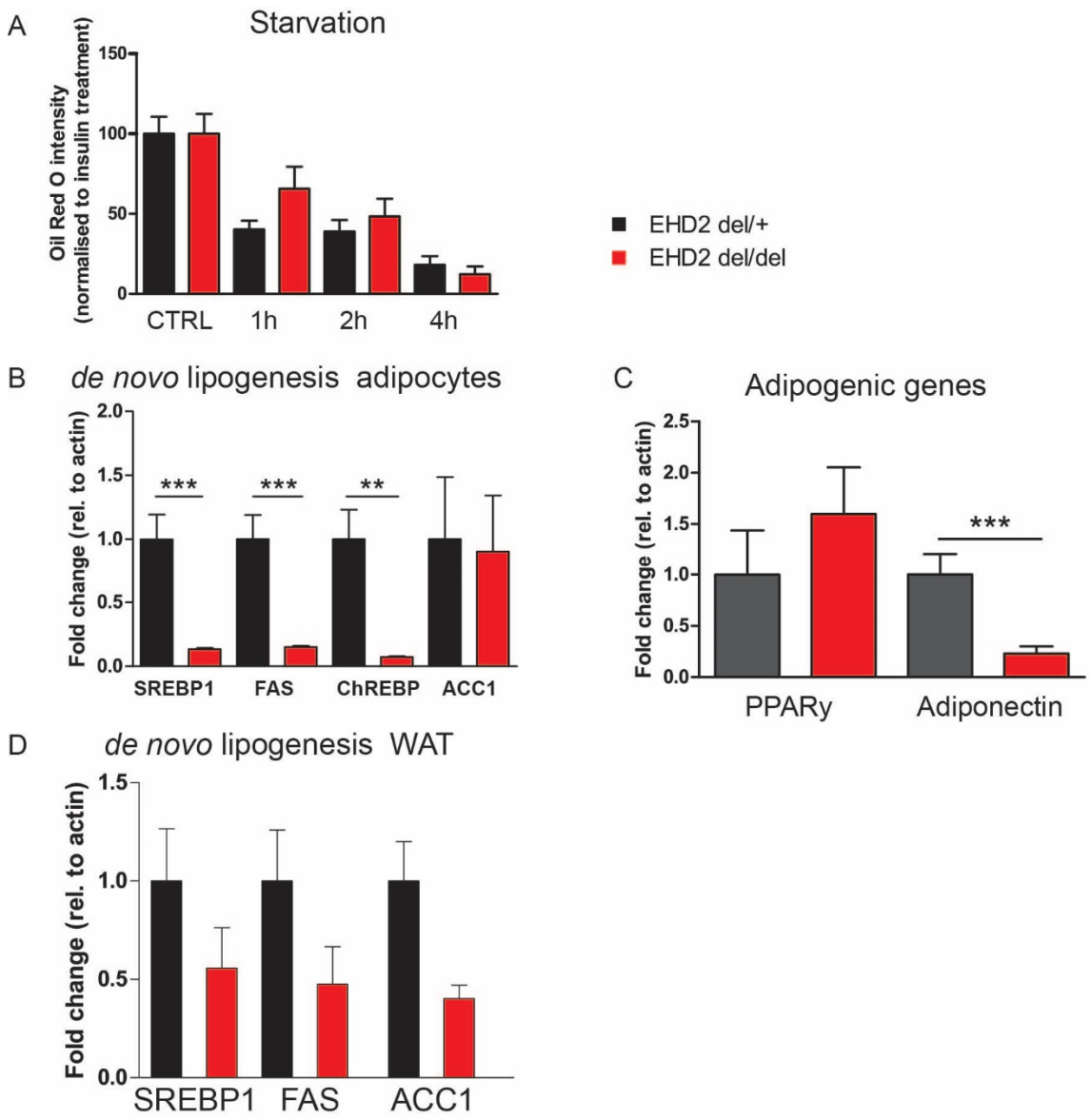

Fig. S5: Cellular investigation of EHD2 del/del adipocytes (related to Fig. 2)

A Differentiated EHD2 del/+ and EHD2 del/del adipocytes were starved for 1-4h and Oil Red O staining was applied (n(EHD2 del/+ = 53/3; n(EHD2 del/del) = 50/3).

B-C Gene expression analysis of genes involved in *de novo* lipogenesis (B) or adipogenic genes (C) in EHD2 del/+ and del/del differentiated adipocytes (n = 8).

D Gene expression analysis of genes involved in *de novo* lipogenesis (n = 5).

Column bars show mean + SE, t-test or Mann Withney U test was used to calculate significance, ** P<0.001, *** P<0.0001.

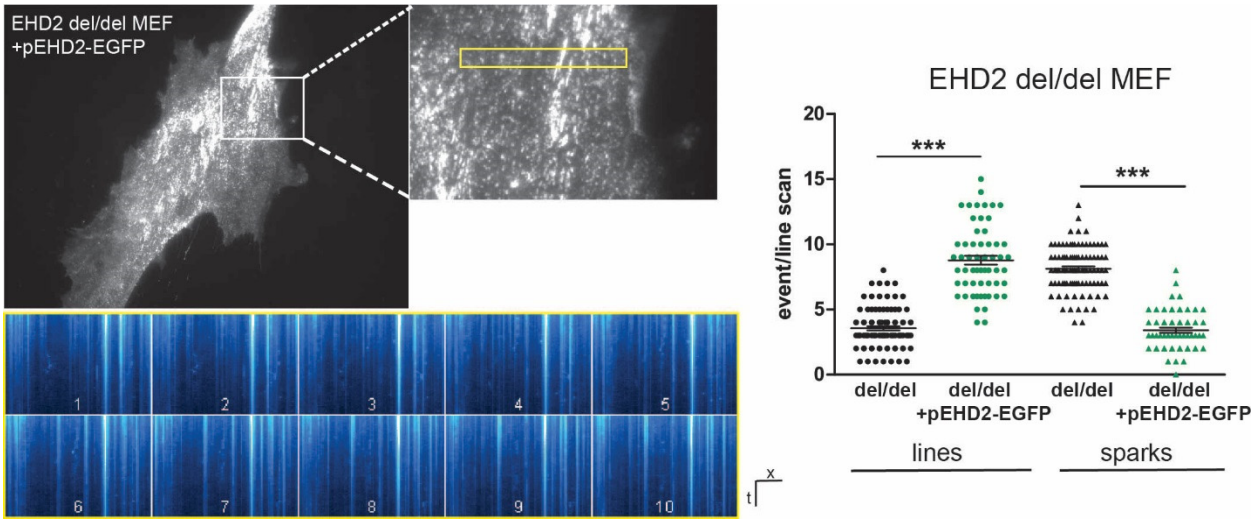

Fig. S6: Caveolar mobility in EHD2 del/del MEFs (related to Fig. 4)

TIRF live-imaging in EHD2del/del MEFs transfected with pEHD2-EGFP and pCav1-EGFP (1:1) to investigate single caveolae movement by TIRF live imaging. Non-moving caveolae correspond to vertical lines within the line scan, moving caveolae can be related to single sparks (B, n = 30, graph illustrates each replicate with mean +/- SE, t-test was used to calculate significance). See also Movie S4.
Plots indicate each replicate from maximal to minimum value with mean, t-test or Mann Withney U test were used to calculate significance, *** P<0.0001.

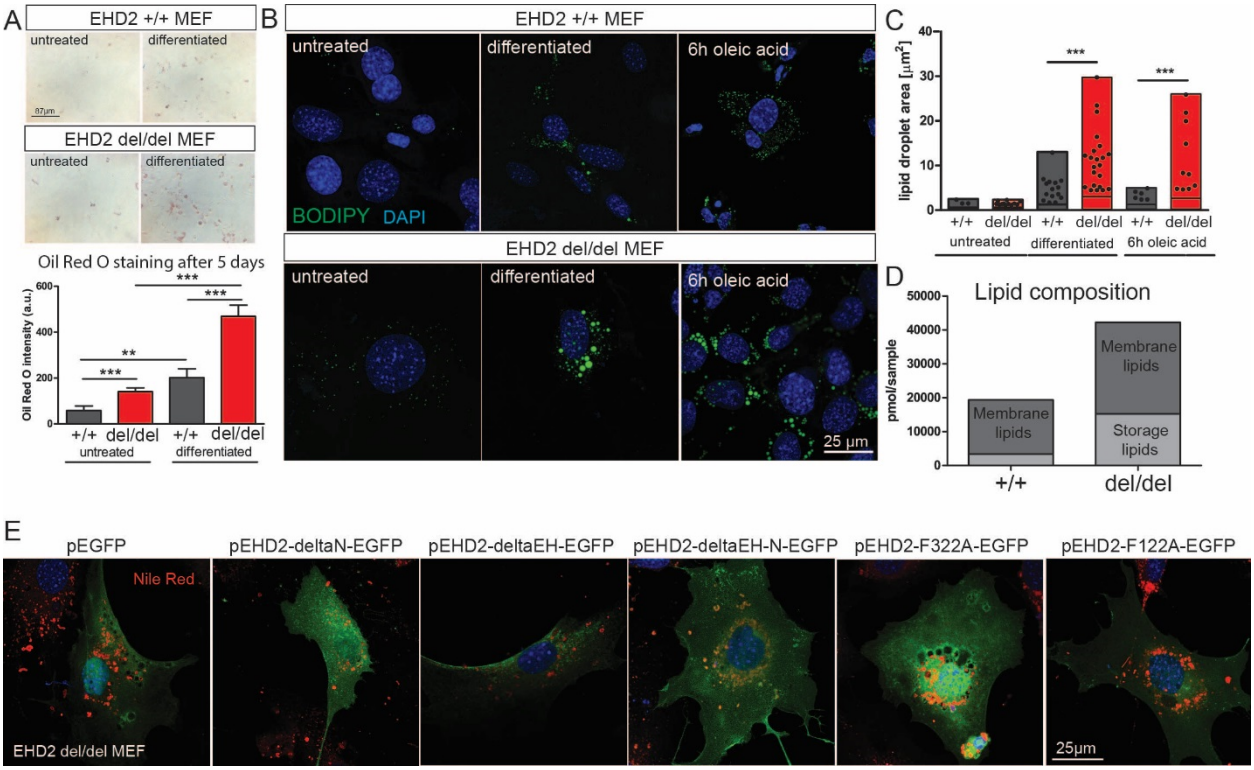

Fig. S7: Caveolar mobility in EHD2 del/del MEFs (related to Fig. 5)

A Oil Red O staining of EHD2 +/+ and del/del MEFs untreated or treated with adipocyte differentiation medium (untreated: n(+/+) = 21/3, n(del/del) = 28/4); differentiated: n(+/+) = 37/3, n(del/del) = 55/4).

B-C LD analysis after 5 days of differentiation or 6 h of oleic acid in EHD2 MEFs by BODIPY staining (D, untreated: n(+/+) = 61/2, n(del/del) = 139/4); differentiated: n(+/+) = 148/3, n(del/del) = 200/4; oleic acid: n(+/+) = 146/3, n(del/del) = 217/3).

D Lipid composition analysis of MEFs differentiated for 5 days, 120,000 cells were analyzed for each experiment (n = 3).

E EHD2 del/del MEFs were transfected with different EHD2 constructs and lipid droplet size was analyzed after 6h oleic acid treatment.

Box plots indicate each replicate from maximal to minimum value with mean, column bar graphs show mean + SE, t-test or Mann Withney U test were used to calculate significance, ** P<0.001, *** P<0.0001.

918 **References SI**

919 1. Cham BE, Knowles BR (1976) A solvent system for delipidation of plasma or serum without
920 protein precipitation. *J Lipid Res* 17:176–181.

921 2. Mehlem A, Hagberg CE, Muhl L, Eriksson U, Falkevall A (2013) Imaging of neutral lipids by oil red
922 O for analyzing the metabolic status in health and disease. *Nat Protoc* 8(6):1149–1154.

923 3. Kärgel E, et al. (1996) Candida maltosa NADPH-cytochrome P450 reductase: cloning of a full-
924 length cDNA, heterologous expression in Saccharomyces cerevisiae and function of the N-
925 terminal region for membrane anchoring and proliferation of the endoplasmic reticulum. *Yeast*
926 12(4):333–348.

927 4. Wilkinson DD (1993) In situ Hybridization. A Practical Approach. *Genet Res* 61(03):234.

928 5. Dubikovskaya E, Chudnovskiy R, Karateev G, Park HM, Stahl A (2014) Measurement of long-chain
929 fatty acid uptake into adipocytes. *Methods Enzym* 538(1):107–134.

930

931

932